

Conical Probe Calibration and Wind Tunnel Data Analysis of the Channeled Centerbody Inlet Experiment

A Cooperative Education Experience Assignment & Senior Project

presented to

the Faculty of the Aerospace Engineering Department

California Polytechnic State University, San Luis Obispo

In Partial Fulfillment

of the Requirements for the

Degree of Bachelor of Science

Samson Siu Truong

Spring 2011

Conical Probe Calibration and Wind Tunnel Data Analysis of the Channeled Centerbody Inlet Experiment

Samson S. Truong*

NASA Dryden Flight Research Center, Edwards, CA, 93523

For a multi-hole test probe undergoing wind tunnel tests, the resulting data needs to be analyzed for any significant trends. These trends include relating the pressure distributions, the geometric orientation, and the local velocity vector to one another. However, experimental runs always involve some sort of error. As a result, a calibration procedure is required to compensate for this error. For this case, it is the misalignment bias angles resulting from the distortion associated with the angularity of the test probe or the local velocity vector. Through a series of calibration steps presented here, the angular biases are determined and removed from the data sets. By removing the misalignment, smoother pressure distributions contribute to more accurate experimental results, which in turn could be then compared to theoretical and actual in-flight results to derive any similarities. Error analyses will also be performed to verify the accuracy of the calibration error reduction. The resulting calibrated data will be implemented into an in-flight RTF script that will output critical flight parameters during future CCIE experimental test runs. All of these tasks are associated with and in contribution to NASA Dryden Flight Research Center's F-15B Research Testbed's Small Business Innovation Research of the Channeled Centerbody Inlet Experiment.

Nomenclature

$CCIE$	=	Channeled Centerbody Inlet Experiment
CFD	=	Computational Fluid Dynamics
C_s	=	Static Pressure Coefficient
$C_{s\alpha}$	=	Angle of Attack Static Pressure Coefficient
$C_{s\beta}$	=	Sideslip Angle Static Pressure Coefficient
C_t	=	Total Pressure Coefficient
$C_{t\alpha}$	=	Angle of Attack Total Pressure Coefficient
$C_{t\beta}$	=	Sideslip Angle Total Pressure Coefficient
C_α	=	Angle of Attack/Pitch Pressure Coefficient
C_{α_0}	=	α - Pitch Coefficient Offset
C_β	=	Sideslip Angle/Yaw Pressure Coefficient
C_{β_0}	=	β - Pitch Coefficient Offset
$DFRC$	=	Dryden Flight Research Center
M	=	Mach Number
$MSFC/ARF TWT$	=	George C. Marshall Space Flight Center Aerodynamic Research Facility 14 × 14-inch Trisonic Wind Tunnel
$NASA$	=	National Aeronautics and Space Administration
P_a	=	Average of Probe Static Pressures
P_o	=	Wind Tunnel Total Pressure, psi
P_s	=	Wind Tunnel Static Pressure, psi
P_1	=	Probe Total Pressure Measured behind Normal Shock at Cone Apex, psi
P_2	=	Probe Static Pressure to the right of P_1 , psi
P_3	=	Probe Static Pressure below P_1 , psi
P_4	=	Probe Static Pressure to the left of P_1 , psi
P_5	=	Probe Static Pressure above P_1 , psi

* Student Trainee Engineer Co-op, Aerodynamics and Propulsion Branch

Q_{bar}	=	Pseudo/Probe Dynamic Pressure, psi
$Q_{bar - true}$	=	True Dynamic Pressure, psi
<i>RTF</i>	=	Real-Time Fortran
<i>SBIR</i>	=	Small Business Innovation Research
\vec{V}	=	Local Velocity Vector
X_p	=	X-axis of Probe Coordinate System
Y_p	=	Y-axis of Probe Coordinate System
Z_p	=	Z-axis of Probe Coordinate System
α	=	Angle of Attack/Pitch Angle, deg
α_o	=	Vertical Misalignment Angle with Probe Rotated 0° and 180°, deg
β	=	Sideslip Angle/Yaw Angle, deg
β_o	=	Vertical Misalignment Angle with Probe Rotated ± 90°, deg
γ	=	Ratio of Specific Heats
δ	=	Uncertainty
θ	=	Pitch Angle, deg
φ	=	Roll Angle, deg

I. Introduction

SUPERSONIC and hypersonic vehicles require inlets with an efficient geometric design that would provide suitable air mass flow into its engines for better low Mach number flight operations. At low supersonic conditions, inlets must be able to provide a substantial amount of transonic airflow in order to meet the engines' demand. As a result, a large inlet throat area is required to fulfill this requirement. This could potentially allow for higher efficiency engine combined cycle propulsion systems, such as the Rocket-Based Combined Cycle (RBCC) and the Turbine-Based Combined Cycle for supersonic cruise or hypersonic acceleration. Research into this area is currently underway with the Channeled Centerbody Inlet Experiment (CCIE), as seen in Fig. 1, at the NASA Dryden Flight Research Center in conjunction with the TechLand Research Incorporation through NASA's Small Business Innovation Research (SBIR) contract.¹

The overall objective of the CCIE research is to investigate the off-design performance of a supersonic inlet with a variable geometry at varying Mach test points. The two primary factors that researchers hope to derive from this study is the inlet flow of both the channeled centerbody and the equivalent area smooth centerbody and how well the flight results compare to the CFD calculations. The channeled centerbody, shown in Fig. 2a, has grooved channels along the centerbody to enhance flight at off-design conditions. These grooves or channels in the centerbody allow for additional throat area to increase the amount of mass flow coming into the inlet during off-design flight. The benefit of having these grooves results in lower internal compression, which allows an aircraft designer to select a mixed-compression inlet configuration often used for high supersonic and hypersonic applications due to its high total pressure recovery and desired high-speed cruise performance. The equivalent smooth centerbody, shown in Fig. 2b, however, has no grooves. The absence of these grooves means that the throat area is smaller and aircraft designers must choose an inlet with high internal compression in order to provide the amount of mass flow the engine needs at off-design conditions. This option means the designer has to risk the high probability of inlet unstart and low operability since this type of inlet with a fixed-geometry requires overspeeding.¹⁻² With flight testing, researchers hope to find out the overall performance of the channeled centerbody and how it compares to the equivalent smooth centerbody. It should be noted that TechLand's concept is a translating channeled centerbody capable of changing the cross-sectional area geometry, while the



Figure 1. The Channeled Centerbody Inlet Experiment (CCIE) is shown here as the gold structure mounted underneath the black Propulsion Flight Test Fixture (PFTF), which in turn is attached to the F-15D centerline pylon through two suspension lugs so that all the loads are transferred to the aircraft.

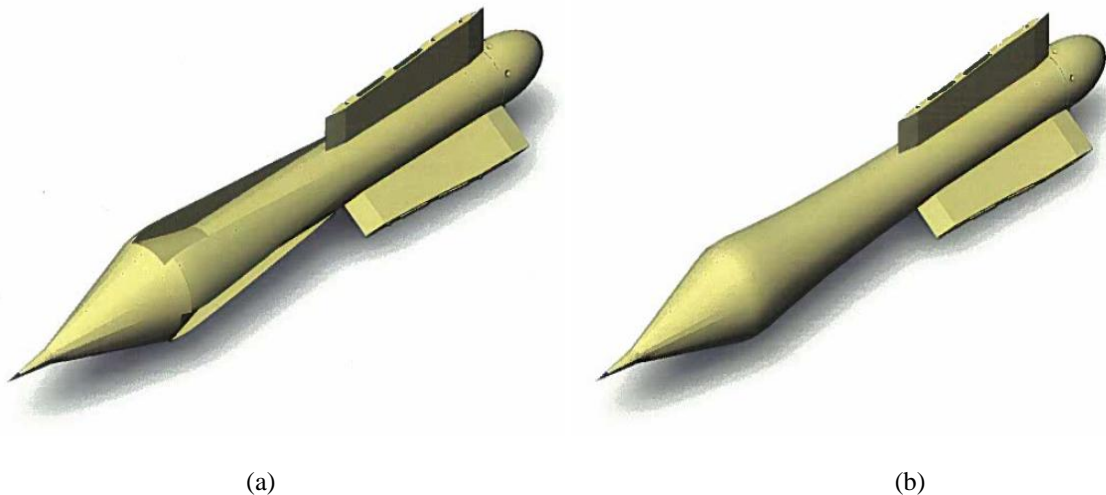


Figure 2. The channeled centerbody (a) and the equivalent smooth centerbody (b) are two of the centerbodies that will be tested for the Channeled Centerbody Inlet Experiment (CCIE).³ Notice that the channeled centerbody has grooves providing more inlet area as opposed to the equivalent smooth centerbody. The channeled centerbody was designed ideally for Mach 1.5 conditions.

one being tested at NASA DFRC is a fixed geometry design. If the flight results provide results as expected, the channeled centerbody inlet concept could potentially be implemented for both commercial and space applications in the near future, ranging from supersonic transports to space-access vehicles.

Prior to any flight testing, one of the tests that prepared the CCIE was a wind tunnel test that obtained data for the 5-hole pressure probes, 4 static and 1 total, located near the nose cone apex, shown in Fig. 3 mounted in the test section. In addition, the conical probe has a 16° cone semivertex or half-angle. The wind tunnel test was conducted in June 2010 at the George C. Marshall Space Flight Center Aerodynamic Research Facility 14×14 -inch Trisonic Wind Tunnel (MSFC/ARF TWT), which recently upgraded its facility with a new data acquisition and tunnel control system. The MSFC/ARF TWT is an intermittent blow-down tunnel where high-pressure air from outside storage tanks flows through a diffuser, a heat exchanger, and into one of two test sections, the transonic or the supersonic test sections. The transonic test section is capable of producing Mach numbers ranging from 0.2 to 2.5, whereas the supersonic test section produces Mach numbers from about 2.7 to 5.0.⁴ For this particular test, the transonic test section was utilized as the CCIE's intent is to investigate off-design low supersonic conditions. The test points included testing at Mach numbers 1.2, 1.3, 1.46, and 1.69, and for each test point, the probe was set at roll angles, ϕ of 0° , 90° , 180° , and -90° with positive angle representing counterclockwise rotation and negative angles representing clockwise rotation. In addition, pitch sweeps were conducted at each Mach condition to gather measurements for angle of attack, α and angle of sideslip, β . The test section is only capable of traversing in the vertical direction and as a result, sideslip had to be measured as pitch maneuver, not a yaw horizontal maneuver. The wind tunnel test resulted in data that was used later for calibration of flow angularity in the pitch and yaw planes as well as the Mach number values that the pressure probes were reading.⁵

During the wind tunnel test of the CCIE's 5-hole pressure probe, it was not expected that the test article would remain stationary at one set location and neither the local velocity vector will be aligned, causing variations in the positioning of the two. Small angularities contributed to the misalignment of either the probe or the local velocity vector and therefore,

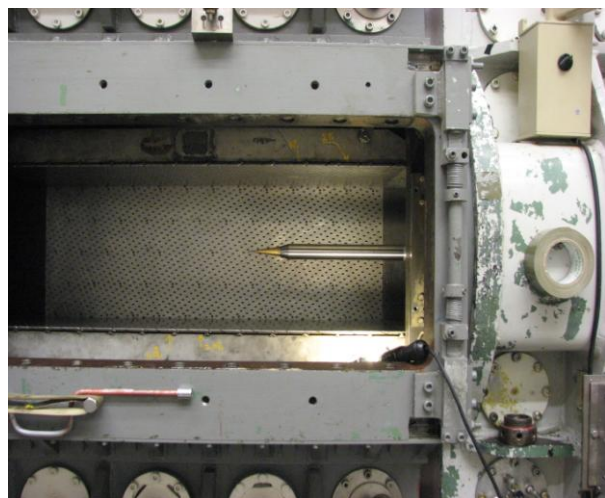


Figure 3. The nose apex of the CCIE is where the 5-hole pressure probe is located and is mounted here in the MSFC/ARF TWT transonic test section.

creates an angular bias that needs to be addressed in the calibration.⁶ As a result, calibration correction of the wind tunnel data for all the Mach number test points needs to be performed in order to determine the relationships between the measured pressures, the probe's geometric orientation, and the local velocity vector. The conical calibration and error reduction process of the CCIE wind tunnel data will produce calibration graphs from which they could be compared to one another to derive any significant trends amongst pressure and angular parameters in the low supersonic regime.

II. Conical Probe Calibration Wind Tunnel Data Analysis & Procedures

The conical probe calibration of the CCIE will consist of several major steps, each of which is critical to the accuracy of the outcome of the calibration. These steps include identifying the key probe parameters and a coordinate system for reference purposes, calculating pressure coefficients of interest to the calibration, the conical calibration process itself detailing how misalignments are calculated and how they are dealt with, and the error and uncertainty analysis post-calibration process. Eventually, the calibrated data and its maps will be used to construct an in-flight RTF code to output desired data in real-time during the CCIE's experimental flight on the F-15B research aircraft.

A. Establish the Probe Parameters and the Coordinate System

Prior to performing the calibration and error reduction, multiple parameters need to be defined in order to have a clear understanding of how to perform the calculations. First, the CCIE multi-hole pressure probes have to be labeled for reference purposes. This particular multi-hole probe has 5 ports, one measuring the total pressure and the other four measuring the static pressure. In Fig. 4, the total pressure port is located in the center amongst the other ports and is designated as P₁. The other ports surrounding P₁ are the static pressure ports. Starting at the right of P₁ and going clockwise, the ports are labeled as P₂, P₃, P₄, and P₅. The pressure measurements from these ports will allow non-dimensional pressure coefficients to be calculated later on. Utilizing a multi-hole pressure probe, also called an impact probe, allows more data collection capability than a standard pitot probe as it now could measure the direction of the flow velocity in three dimensions.

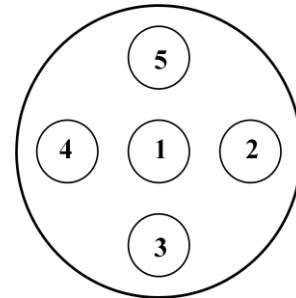


Figure 4. Looking head on, the CCIE multi-hole pressure probe is arranged in this manner for roll angle $\phi = 0^\circ$. The probe, P₁ measures the total pressure, while the remaining probes P₂, P₃, P₄, and P₅ measure the static pressure.

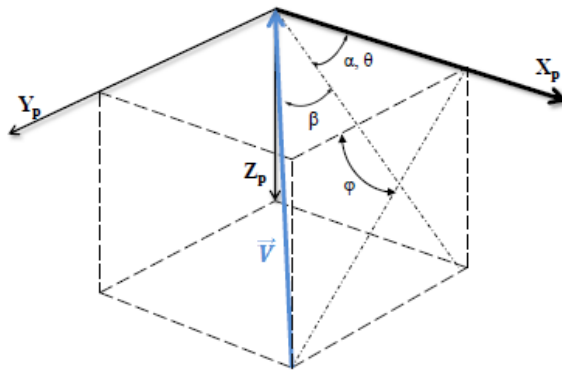


Figure 5. The probe coordinate system is illustrated above with the probe aligning along the X_p-axis. The four angles of interest, angle of attack, α , sideslip angle, β , pitch angle, θ , and roll angle, ϕ are shown here and help in determining the orientation of both the probe and the local velocity vector.

In order to establish any angular parameters, such as angle of attack and roll angle, the probe's position needs to be identified with a coordinate system. During the wind tunnel test and data collection, the probe's position is assumed to be fixed in space. The velocity vector's orientation will be measured with respect to the probe's fixed coordinate system. In Fig. 5, the probe coordinate system is shown with axes X_p, Y_p, and Z_p with the probe aligned along the X_p-axis. The probe tip meets with the incoming local velocity vector, \vec{V} at the origin. Several angles that indicate the position of the probe in relation to the local velocity vector include angle of attack, α , sideslip angle, β , pitch angle, θ , and roll angle, ϕ . The angle of attack or the pitch angle is the angle that the probe makes with respect to the oncoming flow about the Y_p-axis. The sideslip angle or the yaw angle is the angle that the probe makes with the local velocity vector about the Z_p-axis.⁷ Finally, the roll angle is the angle that the probe twists about its centerline on the X_p-axis.

B. Calculate the Pressure Coefficients

With the pressure ports identified, an established coordinate system, and angular parameters defined, the data obtained from these independent variables can be used to determine the unknown dependent variables.⁸ These dependent variables consist of mostly pressure coefficients, which are later plotted against angles of interests and other pressure coefficients to determine behavioral trends in pressure due to different pitch and roll angles at a particular Mach number. Pressure coefficients are significant as they describe the relative pressures about a point, in this case, the probe in a fluid flow field. To determine these pressure coefficients, one variable needs to be calculated that will assist in non-dimensionalizing all of the pressure coefficient variables. This variable is the average probe static pressure, P_a and is equal to the arithmetic mean of the four measured static pressures on the multi-hole probe. It can be calculated as

$$P_a = \frac{1}{4}(P_2 + P_3 + P_4 + P_5). \quad (1)$$

The first pressure coefficient to be calculated is C_α , the angle of attack or the pitch pressure coefficient. During wind tunnel measurements of the multi-hole pressure probe, C_α is associated with roll angles of $\phi = 0^\circ$ and $\phi = 180^\circ$. By looking at the probe's orientation in Fig. 4, these two roll angles align with pressure probes P_1 , P_3 , and P_5 . Therefore, C_α was calculated as the difference between the two static pressures non-dimensionalized by the difference between the total and average static pressures or simply as

$$C_\alpha = \frac{P_3 - P_5}{P_1 - P_a}. \quad (2)$$

The non-dimensionalization by the denominator, $P_1 - P_a$ in Eq. 2 is actually the pseudo or the probe dynamic pressure based on initial measured pressures and can be represented as Q_{bar} . Replacing the denominator in Eq. 2 with the freestream dynamic pressure gives the revised C_α formula in Eq. 3 as

$$C_\alpha = \frac{P_3 - P_5}{Q_{bar}}. \quad (3)$$

The MSFC/ARF TWT's probe holder cannot traverse in the horizontal direction and as a result, data collection for sideslip maneuvers involves the probe being rotated at roll angles of $\phi = 90^\circ$ and $\phi = -90^\circ$. Subsequently, the sideslip angle or the yaw pressure coefficient, C_β was calculated in the same manner, this time along the horizontal axis probes, P_1 , P_2 , and P_4 as shown here in Eq. 4 as

$$C_\beta = \frac{P_4 - P_2}{Q_{bar}}. \quad (4)$$

The total pressure coefficient, C_t is the ratio between the difference in total pressures of the probe, P_1 and the wind tunnel freestream condition, P_o and the freestream dynamic pressure, Q_{bar} . This relation is represented in Eq. 5 as

$$C_t = \frac{P_1 - P_o}{Q_{bar}}. \quad (5)$$

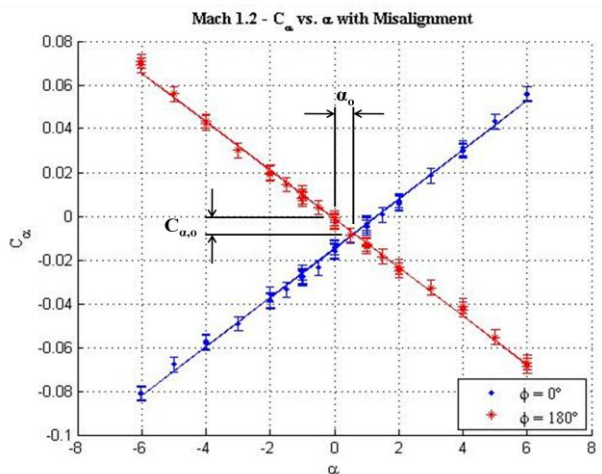
Similarly, the static pressure coefficient, C_s was calculated as the difference between the difference in the total pressure of the probe, P_1 and the wind tunnel static pressure, P_s non-dimensionalized by the freestream dynamic pressure, Q_{bar} . Subtracting out P_s eliminates the static pressure component of the probe total pressure. Thus, C_s was written in Eq. 6 as

$$C_s = \frac{P_1 - P_s}{Q_{bar}}. \quad (6)$$

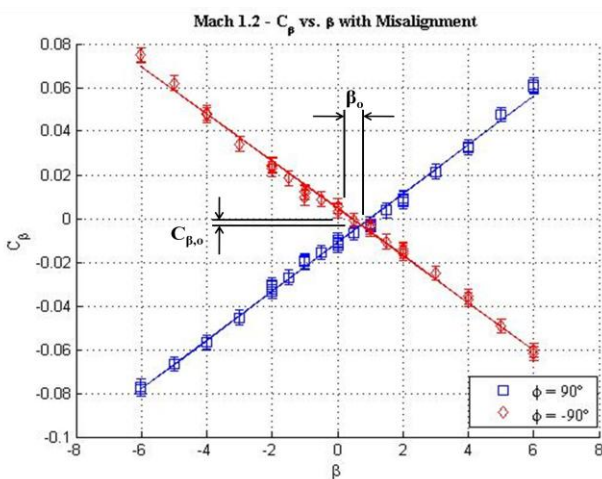
With all of the necessary pressure coefficients calculated, relationships were established between other parameters of interest, such as angle of attack and sideslip angle throughout the calibration process.

C. Determine the Vertical Misalignments

Data collection for angle of attack and sideslip angle were both gathered from the MSFC/ARF TWT test as a vertical pitch maneuver since the probe holder in the wind tunnel was not able to traverse in the horizontal direction. Therefore, the discussion here will focus only on the vertical misalignment case as opposed to the horizontal misalignment case. To assume that the probe is perfectly aligned with the flow field is an assumption that should never be made. In order to visualize the misalignment, plots were created for both the angle of attack and sideslip angle cases by plotting them with their respective dependent variable angle of attack and sideslip pressure



(a)



(b)

Figure 6. For the Mach 1.2 test point, pressure coefficients, C_α and C_β are plotted with their corresponding vertical pitch angles, α and β , respectively. C_α values at $\phi = 0^\circ$ and $\phi = 180^\circ$ as well as C_β values at $\phi = 90^\circ$ and $\phi = -90^\circ$ intersect one another, varying linearly and are about equal in magnitude. α and β values range from $\pm 6^\circ$, while C_α and C_β values ranged from about -0.08 to 0.08. The small pressure coefficient value suggests high dynamic pressure at this particular test point.

coefficients, C_α and C_β . This was done for each of the Mach test points of 1.2, 1.3, 1.46, and 1.69. For simplicity purposes, graphs at Mach 1.2 will be displayed here, while the remaining test points' graphs could be viewed in the Appendix since their trends are similar.

In Fig. 6a, C_α is plotted against angle of attack, α at roll angles, $\phi = 0^\circ$ and $\phi = 180^\circ$, while in Fig. 6b, C_β is plotted against the sideslip angle, β at roll angles of $\phi = 90^\circ$ and $\phi = -90^\circ$. For both cases, C_α and C_β vary linearly with their respective angles with each data point having an associated error bound to it. Due to the error associated with each data point during the wind tunnel test, the data points are of course not in a perfect straight linear line. As a result, the data points for each roll angle need an associated line of best fit, since in theory the pressure coefficients, C_α and C_β are linearly related to their corresponding angles, α and β . For $\phi = 0^\circ$, the line of best fit for the pressure coefficient, C_α can be calculated as

$$C_{\alpha\phi=0^\circ} = m_1\alpha + C_{\alpha\phi=0^\circ(\alpha=0^\circ)} \quad (7)$$

where m_1 is the slope of the best fit line of C_α at $\phi = 0^\circ$, α is the angle of attack, and $C_{\alpha\phi=0^\circ(\alpha=0^\circ)}$ is the y-intercept of the pressure coefficient when $\alpha = 0^\circ$. Likewise, at $\phi = 180^\circ$, C_α is calculated in Eq. 8 as

$$C_{\alpha\phi=180^\circ} = m_2\alpha + C_{\alpha\phi=180^\circ(\alpha=0^\circ)} \quad (8)$$

with m_2 being the slope of the best fit line. Similarly, the sideslip case in Fig. 6b at $\phi = 90^\circ$ and $\phi = -90^\circ$ can have their lines of best fit for the pressure coefficient, C_β written in Eq. 9 and 10 as

$$C_{\beta\phi=90^\circ} = n_1\beta + C_{\beta\phi=90^\circ(\beta=0^\circ)} \quad (9)$$

$$C_{\beta\phi=-90^\circ} = n_2\beta + C_{\beta\phi=-90^\circ(\beta=0^\circ)} \quad (10)$$

where n_1 and n_2 are the slopes of the best fit lines for $C_{\beta\phi=90^\circ}$ and $C_{\beta\phi=-90^\circ}$, respectively. Notice that the best fit lines for C_α at $\phi = 0^\circ$ and $\phi = 180^\circ$ and the best fit lines for C_β at $\phi = 90^\circ$ and $\phi = -90^\circ$ cross one another in Fig. 6a and 6b since the slopes are almost equal in magnitude.

The intersection of the two lines indicates the point where C_α and C_β remains constant regardless of roll angle, as well as dictates the orientation the probe is aligned with the local velocity vector. Also, this point is important as it determines the vertical misalignment angle, α_o and β_o , and the α and β -pitch coefficient offsets, C_{α_o} and C_{β_o} . Remember that the probe in the wind tunnel cannot traverse in the horizontal direction and as a result, β_o and C_{β_o} will be treated as a vertical pitch maneuver. Theoretically, the intersection of the two lines should rest at the origin with α_o and β_o equaling zero and $C_\alpha(0)$ and $C_\beta(0)$ should equal zero as well. This assumes the probe in the wind tunnel is fixed in space and exactly aligned with the local velocity vector, requiring an accurate knowledge of the incoming flow angularity. In addition, the theoretical condition assumes that the probe is symmetrically machined with precision, in which the static pressure ports, P_2 , P_3 , P_4 , and P_5 are drilled equidistance from the probe tip, resulting in equal static pressure values when exactly aligned with the flow field.⁹ However, in reality, these assumptions often do not hold true. As a result, vertical misalignment angles and pitch coefficient offsets are present and need to be calculated. Eventually, the vertical misalignment will be removed from the wind tunnel data to enhance the calibration results. To calculate the vertical misalignment angle, α_o from Fig. 6a, Eq. 7 and Eq. 8 are set equal to each other as this is the intersection point as shown in Eq. 11,

$$m_1\alpha + C_{\alpha_{\varphi=0^\circ}(\alpha=0^\circ)} = m_2\alpha + C_{\alpha_{\varphi=180^\circ}(\alpha=0^\circ)}. \quad (11)$$

Solving for α in Eq. 11 results in the vertical misalignment angle, α_o in Eq. 12

$$\alpha_o = \frac{C_{\alpha_{\varphi=0^\circ}(\alpha=0^\circ)} - C_{\alpha_{\varphi=180^\circ}(\alpha=0^\circ)}}{m_2 - m_1}, \quad (12)$$

which is then substituted into Eq. 13 to solve for the α – pitch coefficient offset, C_{α_o} as shown here

$$C_{\alpha_o} = m_1\alpha_o + C_{\alpha_{\varphi=0^\circ}}. \quad (13)$$

The same procedures could be then applied to calculate the vertical misalignment angle, β_o and its corresponding β – pitch coefficient, C_{β_o} as shown in Fig. 6b. By setting Eq. 9 and Eq. 10 equal to one another as shown in Eq. 14,

$$n_1\beta + C_{\beta_{\varphi=90^\circ}(\beta=0^\circ)} = n_2\beta + C_{\beta_{\varphi=-90^\circ}(\beta=0^\circ)} \quad (14)$$

and solving for β , the vertical misalignment for the sideslip case could be calculated through Eq. 15,

$$\beta_o = \frac{C_{\beta_{\varphi=90^\circ}(\beta=0^\circ)} - C_{\beta_{\varphi=-90^\circ}(\beta=0^\circ)}}{n_2 - n_1}. \quad (15)$$

Substituting β_o into Eq. 16,

$$C_{\beta_o} = n_1\beta_o + C_{\beta_{\varphi=90^\circ}} \quad (16)$$

results in the β – pitch coefficient, C_{β_o} . Both the α and β – pitch coefficient offsets take into account of the aligning errors of the probe in the wind tunnel setup, as well as the asymmetric probe geometry when the probe was machined.

These misalignment calculations were done for each of the four Mach conditions of interest to understand how both the angle of attack and sideslip angle behaved in the wind tunnel compared to the theoretical case. Remember that the theoretical condition assumes perfection in alignment and probe geometry, resulting in absolutely no misalignment and in turn the pitch coefficient offsets would be zero. In Table 1, the vertical misalignment angles and the pitch coefficient offsets for both the angle of attack and the sideslip angle are listed with their corresponding Mach test points. The value for vertical misalignment angles, α_o and β_o vary with Mach number. Mach 1.3's vertical misalignment values of $-1.0^\circ \pm 0.2^\circ$ and $-1.2^\circ \pm 0.2^\circ$ were off the most in magnitude compared to Mach 1.46's case of $0.3^\circ \pm 0.2^\circ$ and $0.4^\circ \pm 0.2^\circ$. The further away the misalignment angle's magnitude is from zero, the more bias there will be from the experimental run. Since it is known that the same probe was used throughout, geometry therefore is consistent with each test, implying that flow conditions and alignment of the probe significantly affected the vertical misalignment values. It should be noted that these wind tunnel tests were

Table 1. The values of vertical misalignment angles, α_o and β_o and their respective pitch coefficient offsets, C_{α_o} and C_{β_o} are shown here at different Mach test point conditions.

MACH	α_o (deg)	C_{α_o}	β_o (deg)	C_{β_o}
1.20	0.6 ± 0.2	-0.008 ± 0.002	0.7 ± 0.2	-0.003 ± 0.001
1.30	-1.0 ± 0.2	-0.005 ± 0.003	-1.2 ± 0.2	-0.0023 ± 0.0003
1.46	0.3 ± 0.2	-0.004 ± 0.001	0.4 ± 0.2	-0.001 ± 0.001
1.69	0.7 ± 0.2	-0.001 ± 0.002	0.8 ± 0.2	-0.001 ± 0.001

conducted over several days and aligning the probe could introduce small bias to the resultant data. For the pitch coefficient offsets, C_{α_o} and C_{β_o} , a descending trend is noted with increasing Mach number. From Eq. 3 and Eq. 4, at high supersonic speeds, the dynamic pressure, Q_{bar} increases due to an increase in both the static and total pressures. The pressure coefficient is related to the inverse of dynamic pressure and as a result, high Mach situations build up dynamic pressure, resulting in low pressure coefficient values.

D. Remove Vertical Misalignment from Data

In order to create calibration maps of the pressure coefficient relation to its angular counterpart, the vertical misalignment angle or angular bias has to be eliminated. Typically, this is done through a series of angular rotations and transformations of the probe about its axes to derive the incoming velocity components prior to rotation.¹⁰ However, this particular calibration won't be looking into detail at the incoming flow, but rather preparing corrected data to be used for in-flight real-time data collection. Removal of the angular bias is quite simple by taking the angle of attack and the sideslip angle and subtracting out its vertical misalignment angle, α_o and β_o , respectively. This results in a corrected value of angle of attack, $\alpha_{corrected}$, and sideslip angle, $\beta_{corrected}$ as shown here in Eq. 17 and Eq. 18:

$$\alpha_{corrected} = \alpha - \alpha_o \quad (17)$$

$$\beta_{corrected} = \beta - \beta_o \quad (18)$$

The C_α and C_β plots with their respective angles are shown below in Fig. 7a and 7b with the misalignment angle removed for Mach 1.2 conditions. This means the intersection of the two roll angle data lines now sits on the α and β -axes at 0° . Essentially, this allows the pressure coefficient values to behave more like the theoretical conditions in the calibrated data.

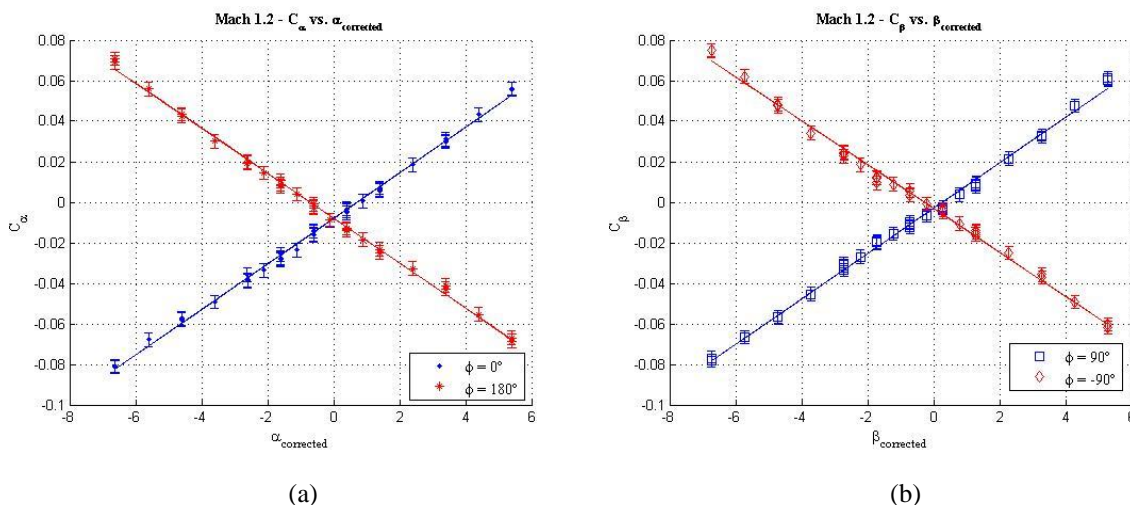


Figure 7. The pressure coefficients, C_α and C_β are plotted with their corresponding vertical pitch angles, α and β , respectively for Mach 1.2 conditions with the vertical misalignment angle removed for each case. Notice the shift at the intersection point as it aligns at $\alpha_{corrected} = 0^\circ$ and $\beta_{corrected} = 0^\circ$.

E. Determine Pitch and Yaw Angle Polynomials

Two important in-flight parameters that need to be monitored during experimental test flights are angle of attack, α , and sideslip angle, β , which are essentially the pitch and yaw motions on an aircraft, respectively. The in-flight real-time Fortran (RTF) script must include equations on how to calculate these two angles, but from Fig. 7, it looks as if there are a set of two equations for both angle of attack at $\varphi = 0^\circ$ and 180° and sideslip angle at $\varphi = 90^\circ$ and -90° . This is because at roll angles, $\varphi = 180^\circ$ and $\varphi = -90^\circ$, the probe is oriented to measure in the negative orientation 180° apart from its positive orientation of $\varphi = 0^\circ$ and $\varphi = 90^\circ$, respectively. Looking at the multi-hole pressure probe arrangement in Fig. 4, to measure the angle of attack, the pressure probe is positioned at $\varphi = 0^\circ$, with pressure ports P_5 located at the top and P_3 located at the bottom. Likewise, measuring sideslip involves positioning the probe at $\varphi = 90^\circ$, with pressure ports P_2 located at the top and P_4 located at the bottom, since the wind tunnel has no horizontal movement capability. At $\varphi = 180^\circ$, angle of attack is measured with pressure ports P_5 and P_3 being switched with one another and this is the same with sideslip measurements at $\varphi = -90^\circ$ with P_2 now measuring at the bottom and P_4 at the top. Since α and β are measured in the negative orientation at $\varphi = 180^\circ$ and $\varphi = -90^\circ$, their data values must be multiplied by negative one. Usually, angular transformations are done to correct the orientation, but since these roll angles are orthogonal, the correction process was simplified. In summary, the pitch angle, θ at $\varphi = 0^\circ$ and $\varphi = 90^\circ$ are equal to α and β , respectively, whereas at $\varphi = 180^\circ$ and $\varphi = -90^\circ$, θ is equal to $-\alpha$ and $-\beta$.

With the negative orientation at roll angles $\varphi = 180^\circ$ and $\varphi = -90^\circ$ accounted for, C_α and C_β are both plotted again for all Mach test points with their respective angles of α and β , this time with both the original and the corrected data with the vertical bias removed. Below in Fig. 8a and 8b, the pressure coefficients are plotted against their corresponding angles for the Mach 1.2 test condition. Notice that for both plots that the corrected data are independent of roll angle. For both the angle of attack and sideslip angle scenarios, their corrected angles with the vertical misalignment eliminated, $\alpha_{\text{corrected}}$ and $\beta_{\text{corrected}}$, are more closely packed together, forming a nice linear trend. From Table 1, it can be inferred that the Mach test points with lower vertical misalignment values of α_o and β_o will have both their original and corrected α and β values closer in proximity to each other, such as Mach 1.46 as opposed to Mach 1.3 with the highest values of α_o and β_o . The plots for the Mach 1.3, 1.46, and 1.69 case could be viewed in the Appendix for reference.

The linear trend produced by the graphs in Fig. 8 between the pressure coefficients and the corrected α and β data is much better than that of the original data, but the corrected data is still slightly off as some data points don't necessarily follow in a straight line. Knowing that both the pressure coefficients, C_α and C_β and their respective angles, α and β are linearly related, a line of best fit could therefore be used to represent the theoretical angle of attack and sideslip angle based on the wind tunnel data. By making $\alpha_{\text{corrected}}$ and $\beta_{\text{corrected}}$ the dependent variable in

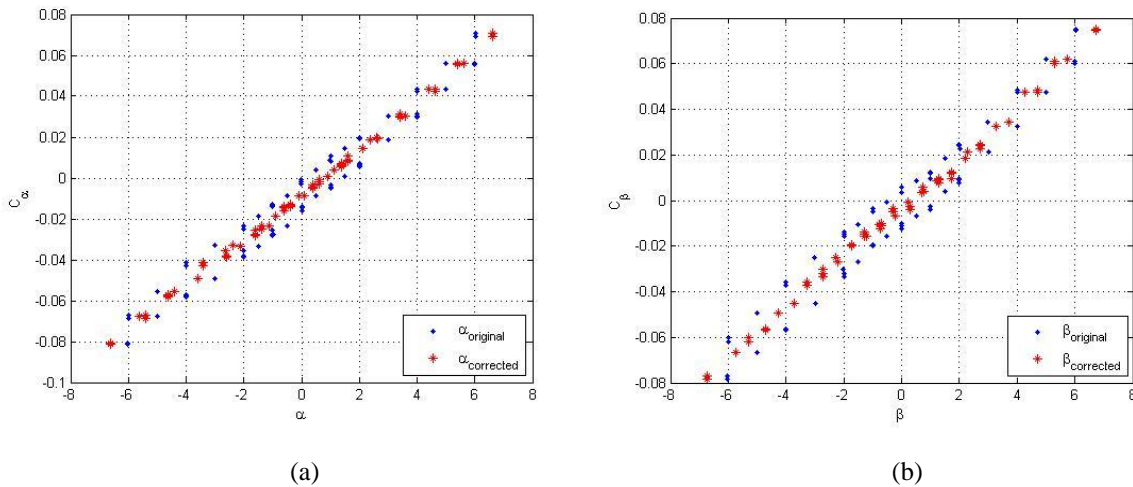


Figure 8. For the Mach 1.2 test point, the pressure coefficients, C_α and C_β are plotted against their respective angles, α and β , with their original data with the misalignment and the corrected data with the misalignment removed. With both the corrected data taking into account of the negative orientation at roll angles $\varphi = 180^\circ$ and $\varphi = -90^\circ$, the pressure coefficient relationship with their pitch and yaw angles are now essentially independent of roll angle and vary linearly.¹¹

the graphs in Fig. 8, solving for these dependent variables is simple by using MATLAB's data fitting tool. Figure 9 displays the line of best fit between the corrected angle of attack and sideslip angle with their corresponding pressure coefficients at Mach 1.2 conditions.

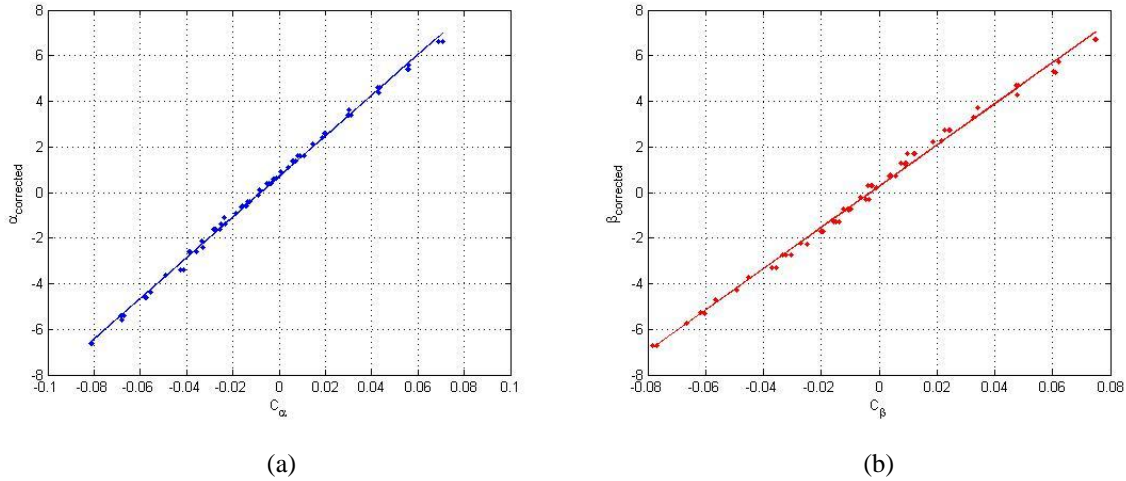


Figure 9. The lines of best fit are shown here between the $\alpha_{\text{corrected}}$ and C_α plot (a) and the $\beta_{\text{corrected}}$ and C_β plot (b). This linear fit curve represents the theoretical angle of attack and sideslip angle equations as a function of pressure coefficients based on the wind tunnel data obtained. These equations will eventually be implemented with the in-flight RTF script as $\alpha = \alpha(C_\alpha)$ and $\beta = \beta(C_\beta)$.

With the aid of MATLAB, the remainder test points had their pitch and yaw angle polynomials calculated at Mach 1.3, 1.46, and 1.69. Table 2 shows the list of angle of attack and sideslip angle equations for each of the associated Mach test points. These equations will be used in conjunction with other equations developed along the way to create the in-flight RTF script for the CCIE. The CCIE's focus is in the supersonic regime primarily between Mach 1.2 and Mach 1.69. The RTF code will eventually have to interpolate the solutions between each equation in order to get the angle of attack and the sideslip angle values that are not exactly right at the calibration Mach test point. This will be furthered discussed in detail later on in this report.

Table 2. The pitch and yaw angle polynomials are shown in this table for each of the Mach number test points. All of these equations were derived based on the linear line of best fit between $\alpha_{\text{corrected}}$ and C_α as well as between $\beta_{\text{corrected}}$ and C_β . These equations are to be utilized in the in-flight RTF code to calculate both the angle of attack and sideslip angle.

MACH	α	β
1.20	$89.1385C_\alpha + 0.7089$	$90.4277C_\beta + 0.2841$
1.30	$94.6015C_\alpha + 0.5037$	$100.0237C_\beta + 0.2179$
1.46	$108.0175C_\alpha + 0.4175$	$112.3877C_\beta + 0.1192$
1.69	$99.9231C_\alpha + 0.1318$	$100.8961C_\beta + 0.0871$

F. Determine Total and Static Pressure Coefficient Polynomials

The total pressure coefficient, C_t and static pressure coefficient, C_s were previously calculated in Eq. 5 and 6. The task now is to find a relationship that relates these two pressure coefficients as a function of the pitch pressure coefficient, C_α and the yaw pressure coefficient, C_β . The procedure for this is similar to the previous section on determining the pitch and yaw coefficient polynomials. The trends in both the total pressure coefficient as well as the static pressure coefficient for all the Mach test conditions will be compared to the theoretical case to see how well the wind tunnel test results did. The resulting wind tunnel results will be then fitted to formulate equations for C_t and C_s that will then be incorporated into the in-flight RTF code.

Figures shown previously at Mach 1.2 had the same behavior at Mach numbers 1.3, 1.46, and 1.69, but plots involving the total and the static pressure coefficient are an exception as they behave a bit differently. The angle of attack total pressure coefficient, $C_{t\alpha}$, and the sideslip angle total pressure coefficient, $C_{t\beta}$, are both plotted in Fig. 10 and Fig. 11 as a function of C_α and C_β , respectively for test points at Mach 1.2, 1.3, 1.46, and 1.69. These side by side comparisons between the test points reveal that the angle of attack total pressure coefficient trend behavior does not stay consistent. Mach 1.2 and Mach 1.46 had a linear fit as opposed to Mach 1.3 and Mach 1.69 with a quadratic fit. For the Mach 1.2 instance in Fig. 10a, the linear fit fell near all the data points and within their error bounds. Mach 1.46 in Fig. 10c deviated from the other Mach numbers as its line of best fit, despite higher order

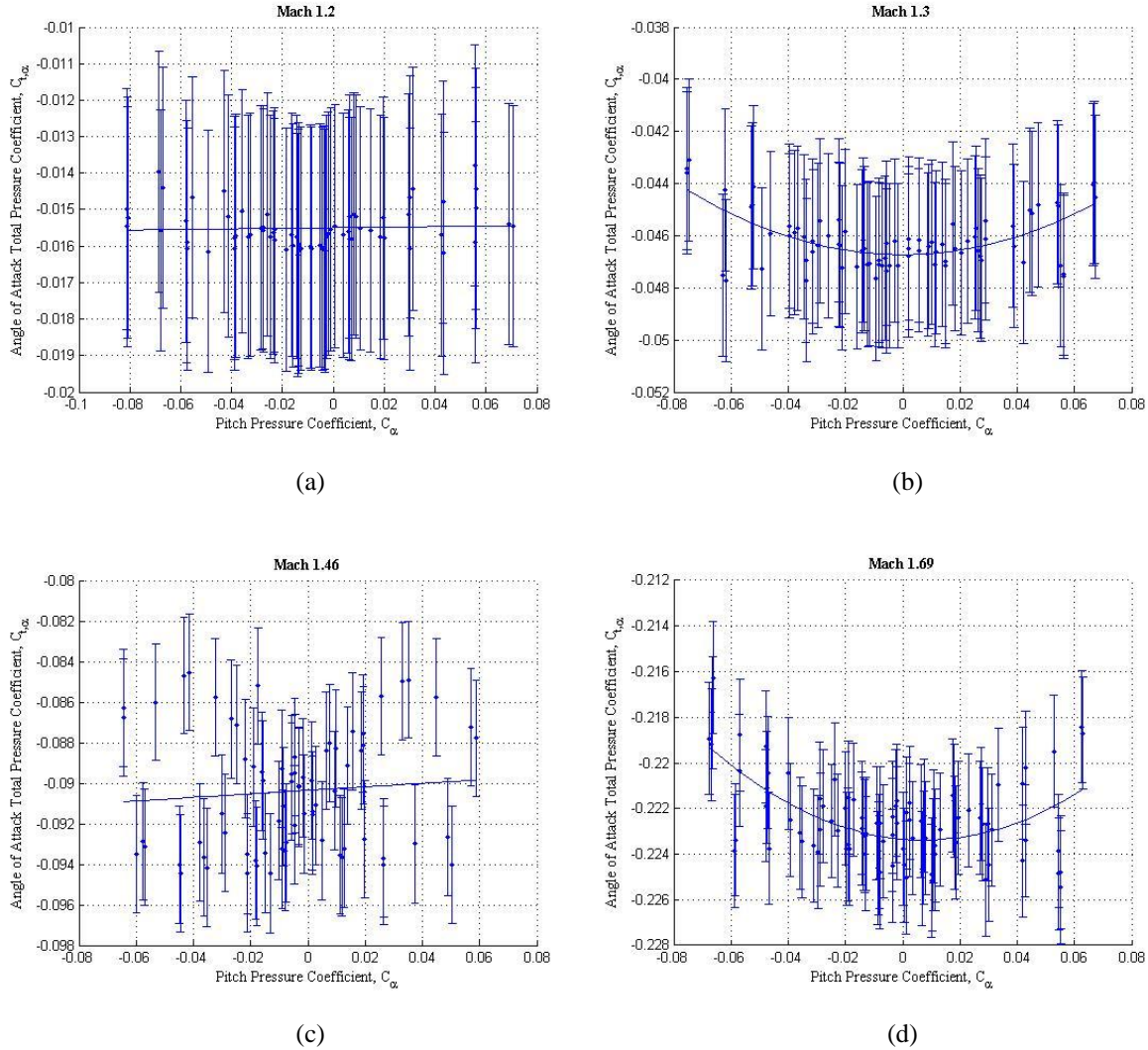


Figure 10. The angle of attack total pressure coefficient, $C_{t\alpha}$ is plotted as a function of the angle of attack pressure coefficient, C_α for test points at Mach 1.2 (a), Mach 1.3 (b), Mach 1.46 (c), and Mach 1.69 (d). C_α values remained consistent for all Mach numbers, ranging from -0.08 to 0.08, while $C_{t\alpha}$ values increase in magnitude with higher Mach numbers, but overall remain close to zero since the total pressure coefficient subtracts out the wind tunnel total pressure, P_0 as seen in Eq. 5. Lines of best fits were obtained for each test point, with Mach 1.46 being the worst of the fits. Higher order fits did not even perform well at this particular test point, but since the range of $C_{t\alpha}$ was small as seen in the y-axis scaling, a first-order fit was acceptable. With the other Mach numbers performing well fitting wise, the Mach 1.46 test point may have encountered either a pressure reading issue with the wind tunnel pressure transducers or a non-uniform flow field.

attempts, had trouble acquiring a noticeable trend. Since C_{t_α} data values at Mach 1.46 only differ from one another by a few thousandths, it was decided a first-order linear fit should work fine. The purpose of the line fitting is not to connect all the wind tunnel data points, but rather obtain a trend that best describes the behavior at that test condition.

The similar behavior observed as seen in Fig. 10 could be seen in Fig. 11 with the sideslip angle total pressure coefficient, C_{t_β} plotted as a function of the yaw pressure coefficient, C_β for all the Mach number test points. Again, Mach 1.2 and 1.46 were fitted linearly, while Mach 1.3 and 1.69 had a quadratic fit. In addition, C_{t_β} values were comparable to that of C_{t_α} . This will help in the approximation of a single total pressure coefficient, C_t value later on when computing the desired flow properties. At Mach 1.2, both lines of best fit for C_{t_α} and C_{t_β} shown in Fig. 10a and Fig. 11a suggest a mean value between -0.015 and -0.016. Mach 1.3 and Mach 1.69 conditions for both the angle of attack and sideslip angle total pressure coefficients showed a decrease in magnitude at the end limits of their pitch and yaw pressure coefficients. Mach 1.46, however, demonstrated a similar behavior as seen in Fig. 10c may have been caused by either a pressure reading issue, a flow disturbance due to a non-uniform flow field, or

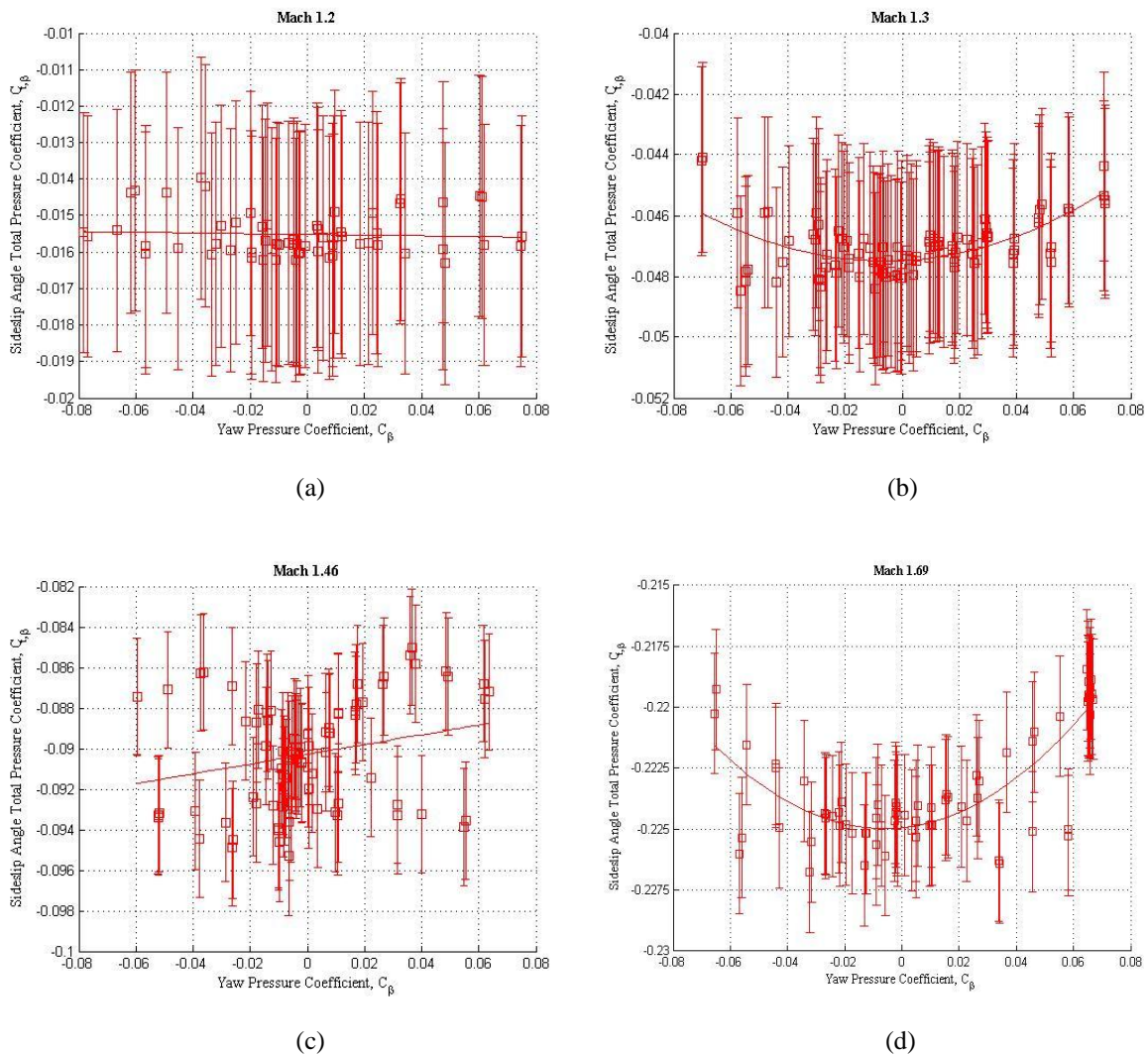


Figure 11. The sideslip angle total pressure coefficient, C_{t_β} is plotted as a function of the angle of attack pressure coefficient, C_α for test points at Mach 1.2 (a), Mach 1.3 (b), Mach 1.46 (c), and Mach 1.69 (d). Notice the similarity in the trends and values between the sideslip angle and angle of attack total pressure coefficient figures.

experiencing a resonating frequency. This will be further looked into later on by the CCIE aerodynamicists.

Static pressure coefficient trends for all the test points resulted in a similar concave down behavior for both the angle of attack and the sideslip angle cases. Below in Fig. 12, the angle of attack static pressure coefficient, $C_{s\alpha}$ is plotted in variation with the pitch pressure coefficient, C_α for all the four Mach test conditions. With increasing Mach number, the freestream wind tunnel static pressure, P_s decreased, while the dynamic pressure increased. From Eq. 6, this resulted in lower values of the static pressure coefficient as the Mach number goes higher. The wind tunnel results have $C_{s\alpha}$ values around a value of one, which is expected based on Eq. 6. Based on Fig. 12 for all test points, slightly lower values of $C_{s\alpha}$ occurred at the low and high ends of C_α . When these graphs were fitted, a quadratic fit was used for Mach 1.2, 1.3, and 1.69, while Mach 1.46 with its steeper concave down trend required a cubic fit for higher accuracy. Much of the data points along with their error bars fell within reach of the lines of best fit. Since these low order fits were capable of matching the angle of attack static pressure coefficient's trends, other higher order fit polynomials were not needed.

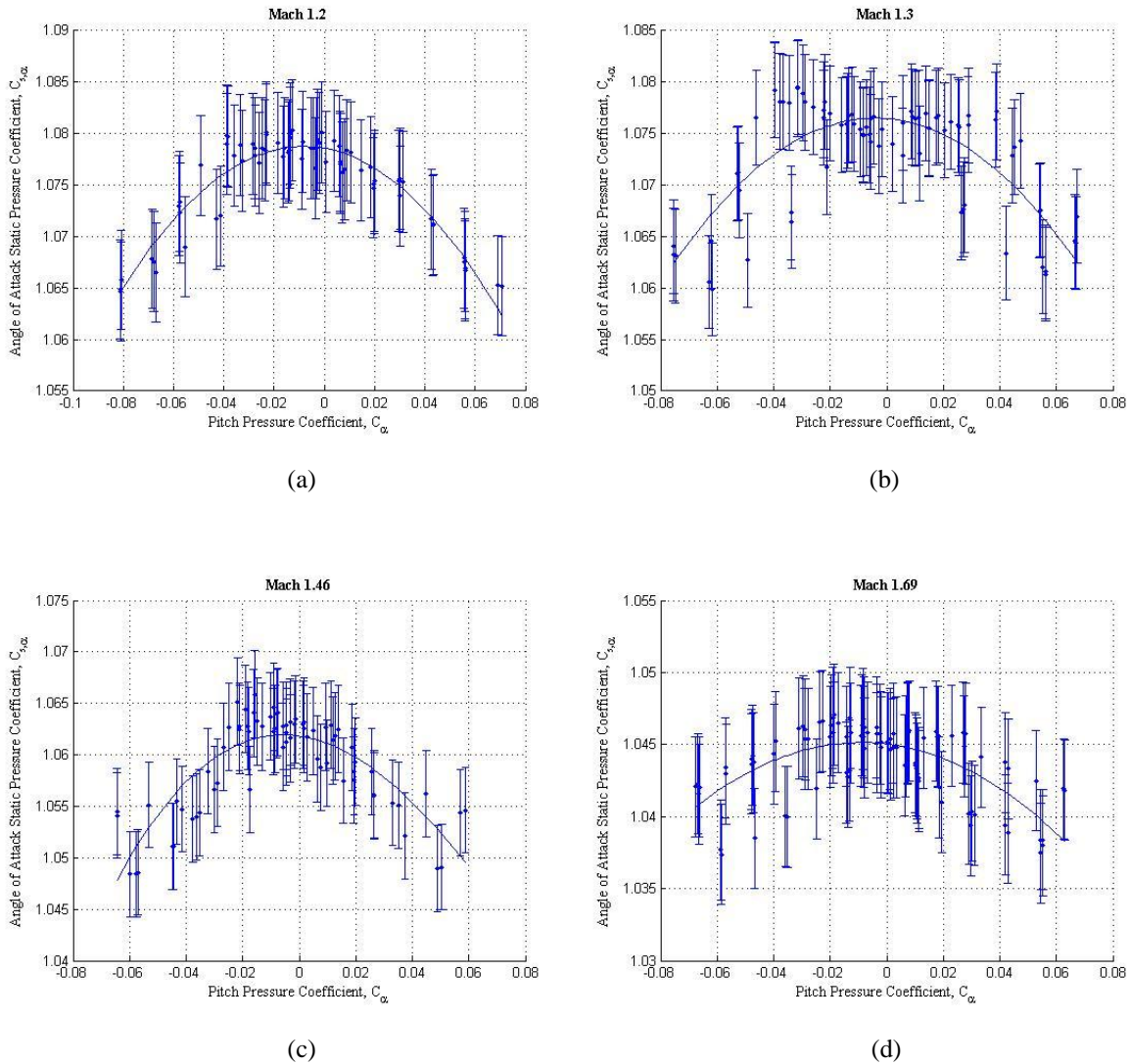


Figure 12. The angle of attack static pressure coefficient, $C_{s\alpha}$ is plotted as a function of the pitch pressure coefficient, C_α for Mach 1.2 (a), Mach 1.3 (b), Mach 1.46 (c), and Mach 1.69 (d). The plots here involving the static pressure coefficient observed a more comparable behavior amongst all the test points with its concave down trend fit. Values of $C_{s\alpha}$ increased with ascending Mach number varying anywhere between 1.03 and 1.095.

Like $C_{s\alpha}$, the sideslip angle static pressure coefficient, $C_{s\beta}$ behaved similarly as plotted in Fig. 13 for all the four Mach conditions as a function of the yaw pressure coefficient, C_β . Trends in the best fit lines and the ranges of values for $C_{s\beta}$ are analogous to that of the angle of attack case. Comparing the angle of attack and the sideslip angle case for the total pressure coefficient plots in Fig. 10 and 11 and the static pressure coefficient plots in Fig. 12 and 13 evidently reveal that regardless of the probe orientation, the values of total pressure coefficient and static pressure coefficient hardly changed between the angle of attack and the sideslip angle scenario. So far, these graphs have been analyzed separately as the total pressure coefficient and the static pressure coefficient cases with respect to their corresponding angular pressure coefficients. Since their data points vary by mere tenths or thousandths of a decimal place, the resulting lines of best fit trends could only be viewed up close. If these coefficients, total and static, were plotted simultaneously on the same graph with their respective pitch and yaw pressure coefficients, C_α and C_β , resultant horizontal linear lines of no slope would represent the values of the total and static pressure coefficients as near 0 and 1, respectively. This distinctive trend could be viewed in Fig. 14. With the same exact behavior seen at every Mach test situation, only Mach 1.2's and Mach 1.46's trends will be shown due to their

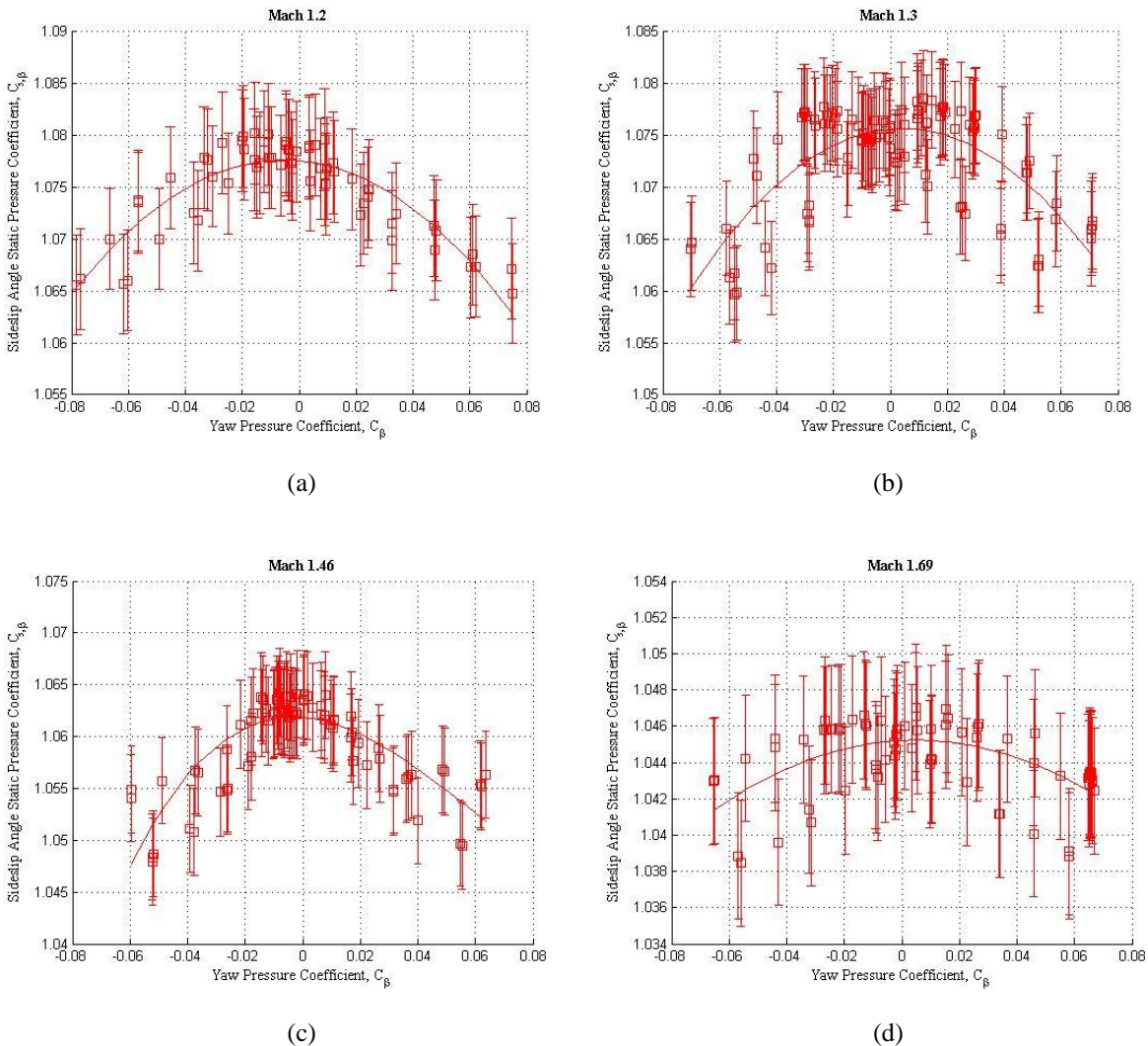


Figure 13. The sideslip angle static pressure coefficient $C_{s\beta}$ is plotted as a function of the yaw pressure coefficient, C_β for Mach 1.2 (a), Mach 1.3 (b), Mach 1.46 (c), and Mach 1.69 (d). For each Mach test point, their figures are close in likeness to that of their counterparts in the angle of attack case in Fig. 12. Mach test points 1.2, 1.3, and 1.69 were fitted with a 2nd order best fit, whereas Mach 1.46 was fitted with a 3rd order trend line.

differing behavior in the total and static pressure coefficient graphs for both the angle of attack and sideslip angle cases. The graphs for Mach 1.3 and Mach 1.69 can be seen in the Appendix for reference. The static and total pressure coefficients, C_s and C_t are plotted together as a function of the pitch and yaw pressure coefficients, C_α and C_β for Mach 1.2 in Fig. 14a and Fig 14b and for Mach 1.46 in Fig. 14c and Fig 14d, respectively. From the figures, there are two distinct horizontal lines, with the static pressure coefficients, $C_{s\alpha}$ and $C_{s\beta}$, aligning a little bit above a value of one due to dominance of the higher total pressure values and the total pressure coefficients, $C_{t\alpha}$ and $C_{t\beta}$, aligning slightly below zero, since $P_1 \neq P_0$ in supersonic conditions due to likely pressure differentials across shockwaves. Even with the multi-hole probe being rotated in the wind tunnel, the independence of roll angle is shown here with all the data point values having nearly identical values.

With this verification that the static and total pressure coefficient are behaving as they are supposed to be from this perspective, the total and static pressure coefficient polynomials for both the angle of attack and sideslip angle instances need to be compiled. These equations will later be used to calculate initial flow properties of interest to verify the calibration procedure thus far and will of course be integrated with the in-flight RTF script.

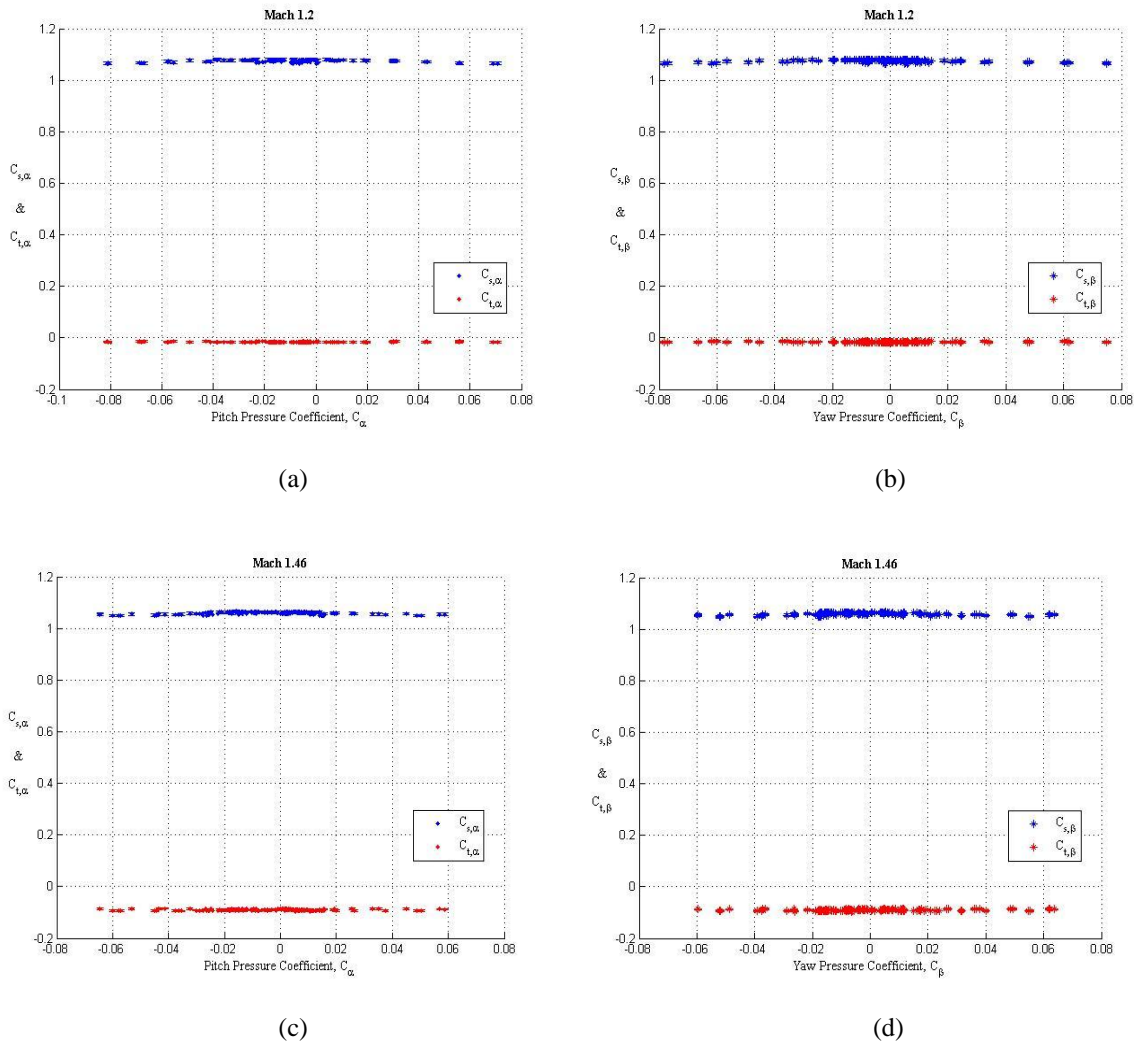


Figure 14. For Mach 1.2 (a & b) and Mach 1.46 (c & d), both their angle of attack and sideslip angle static and total pressure coefficients, $C_{s\alpha}$, $C_{s\beta}$, $C_{t\alpha}$, and $C_{t\beta}$, are plotted with their respective angular pressure coefficients, C_α and C_β . From this different vantage point, one can note the independence of roll orientation in terms of the total and static pressure coefficients for both the angle of attack and sideslip angle situations. Despite Mach 1.2 and 1.46 having differing trends between total and static on a close-up scale, the trends are virtually identical when the two different pressure coefficients are plotted concurrently.

Table 3 displays all the resulting derived polynomial equations for the angle of attack and sideslip angle total and static pressure coefficients for each of the test conditions at Mach 1.2, 1.3, 1.46, and 1.69.

Table 3. For each of the following supersonic test points, the equations for the angle of attack and sideslip angle total and static pressure coefficients, $C_{t\alpha}$, $C_{t\beta}$, $C_{s\alpha}$, and $C_{s\beta}$ were derived based on their lines of best fits for all their trend plots seen in Fig. 10 and 11 for the total pressure coefficient case and Fig. 12 and 13 for the static pressure coefficient case.

MACH	Total & Static Pressure Coefficients	Polynomials
1.20	$C_{t\alpha}$	$(7.9419 \times 10^{-4})C_{\alpha} - 0.015497$
	$C_{t\beta}$	$(-1.0123 \times 10^{-3})C_{\beta} - 0.015517$
	$C_{s\alpha}$	$-2.6378C_{\alpha}^2 - 0.043026C_{\alpha} + 1.0786$
	$C_{s\beta}$	$-2.3004C_{\beta}^2 - 0.023978C_{\beta} + 1.0776$
1.30	$C_{t\alpha}$	$0.43365C_{\alpha}^2 - (1.2153 \times 10^{-4})C_{\alpha} - 0.046727$
	$C_{t\beta}$	$0.38196C_{\beta}^2 + (4.5245 \times 10^{-3})C_{\beta} - 0.047481$
	$C_{s\alpha}$	$-2.7522C_{\alpha}^2 - 0.021851C_{\alpha} + 1.0765$
	$C_{s\beta}$	$-2.7696C_{\beta}^2 - 0.023859C_{\beta} + 1.0756$
1.46	$C_{t\alpha}$	$(8.6243 \times 10^{-3})C_{\alpha} - 0.090352$
	$C_{t\beta}$	$0.024073C_{\beta} - 0.090279$
	$C_{s\alpha}$	$8.5362C_{\alpha}^3 - 3.3971C_{\alpha}^2 - 0.038168C_{\alpha} + 1.0618$
	$C_{s\beta}$	$17.772C_{\beta}^3 - 3.2717C_{\beta}^2 - 0.021265C_{\beta} + 1.0618$
1.69	$C_{t\alpha}$	$0.72013C_{\alpha}^2 - 0.010757C_{\alpha} - 0.22335$
	$C_{t\beta}$	$0.96616C_{\beta}^2 + 0.012028C_{\beta} - 0.22493$
	$C_{s\alpha}$	$-1.3094C_{\alpha}^2 - 0.024019C_{\alpha} + 1.0450$
	$C_{s\beta}$	$-0.78067C_{\beta}^2 + (7.8296 \times 10^{-3})C_{\beta} + 1.04542$

G. Compute Flow Properties

With the measured pressures from the CCIE probe wind tunnel data, initial pressure coefficients were calculated, vertical biases were computed and eliminated from the data, and pitch and yaw angles, as well as total and static pressure coefficient polynomials were derived. The new calibration equations for these various parameters will further contribute in creating calibrated flight properties to be used for uncertainty analysis and comparison with actual future flight data. These properties that need to be analyzed based on their wind tunnel results and calibrated include, total pressure, P_t , static pressure, P_s , Mach number, and the true dynamic pressure, $Q_{bar - true}$. These four parameters will be calculated with respect to angle of attack and sideslip angle, thus there will be two equations and two separate sets of calibrated data for each of these flow properties.

The total pressure could be calculated by simply solving for P_o in the total pressure coefficient in Eq. 5. Since P_o will be solved for both the angle of attack and the sideslip angle instances, the only variable of significant difference

will be the total pressure coefficients, $C_{t\alpha}$ and $C_{t\beta}$. For the angle of attack case, rearranging Eq. 5 results in Eq. 19 as

$$P_{o\alpha} = P_1 - C_{t\alpha} Q_{bar} \quad (19)$$

where $P_{o\alpha}$ is the flow field angle of attack total pressure, P_1 is the CCIE probe total pressure measured, $C_{t\alpha}$ is the angle of attack total pressure coefficient calculated from the equations derived in Table 3, and Q_{bar} is the measured pseudo or probe dynamic pressure in the wind tunnel. Similarly, the sideslip angle total pressure, $P_{o\beta}$ could be calculated in Eq. 20 as

$$P_{o\beta} = P_1 - C_{t\beta} Q_{bar} \quad (20)$$

with $C_{t\beta}$ being the sideslip angle total pressure coefficient. Likewise, calculating the static pressure is the same, only this time by solving for P_s in Eq. 6. This results in Eq. 21 and 22 for the angle of attack and sideslip angle static pressure, $P_{s\alpha}$ and $P_{s\beta}$, respectively as shown here

$$P_{s\alpha} = P_1 - C_{s\alpha} Q_{bar} \quad (21)$$

$$P_{s\beta} = P_1 - C_{s\beta} Q_{bar} \quad (22)$$

where $C_{s\alpha}$ is the angle of attack static pressure coefficient and $C_{s\beta}$ is the sideslip angle static pressure coefficient. With both the total and static pressures known, the calibrated Mach number can be obtained by using the isentropic normal shock relations with the Mach number depending on the total-to-static pressure ratio.¹² The calibrated angle of attack Mach number can be calculated in Eq. 23 as

$$M_\alpha = \left[\left(\frac{2}{\gamma-1} \right) \left(\left(\frac{P_{o\alpha}}{P_{s\alpha}} \right)^{\frac{\gamma-1}{\gamma}} - 1 \right) \right]^{0.5} \quad (23)$$

using the solutions to its respective total and static pressures in Eq. 19 and 21. γ is the ideal ratio of specific heats for air, which is a value of 1.4. Using the results of the sideslip angle total and static pressures from Eq. 20 and 22, the calibrated sideslip angle Mach number is derived using Eq. 24,

$$M_\beta = \left[\left(\frac{2}{\gamma-1} \right) \left(\left(\frac{P_{o\beta}}{P_{s\beta}} \right)^{\frac{\gamma-1}{\gamma}} - 1 \right) \right]^{0.5} . \quad (24)$$

Once the Mach numbers were calculated, the calibrated or true dynamic pressure can be calculated using its compressible flow relation, which is dependent on the static pressure and the Mach number. The true dynamic pressure could be calculated for the angle of attack and the sideslip angle case in Eq. 25 and Eq. 26, respectively,

$$(Q_{bar-true})_\alpha = \frac{1}{2} \gamma P_{s\alpha} M_\alpha^2 \quad (25)$$

$$(Q_{bar-true})_\beta = \frac{1}{2} \gamma P_{s\beta} M_\beta^2 \quad (26)$$

using the calibrated static pressure values calculated in Eq. 21 and 22 and the Mach numbers computed in Eq. 23 and 24. All of these calibrated flow properties will undergo error analysis and will eventually be implemented into the in-flight RTF script that will be discussed later on in this report. With the majority of the calibrated calculations completed, there is still one more variable of importance that needs to be computed prior to performing the uncertainty analysis. This variable is the static-pitot pressure ratio and it will be used to verify the accuracy of the wind tunnel data to its theoretical counterpart.

H. Static-Pitot Pressure Ratio Comparison

The static-pitot pressure ratio, $\frac{P_a}{P_1}$ is the ratio between the average of the measured static pressures to the total pressure, which is measured behind the normal shock at the apex of the conical probe. This ratio is very important in conical flow theory as it will help in determining an initial theoretical estimate of Mach number for the in-flight script, which will in turn output the actual local Mach number based on the measured probe pressures. In order to see how well the wind tunnel results fits with the conical flow theory, plots of the static-pitot ratio were plotted as a function of the pitch angle for each of the Mach test points as shown in Fig. 15. Note angle of attack and sideslip angle were measured as pitch angle as pitch maneuver and both can be represented by the pitch angle, θ . All of the plots exhibit a

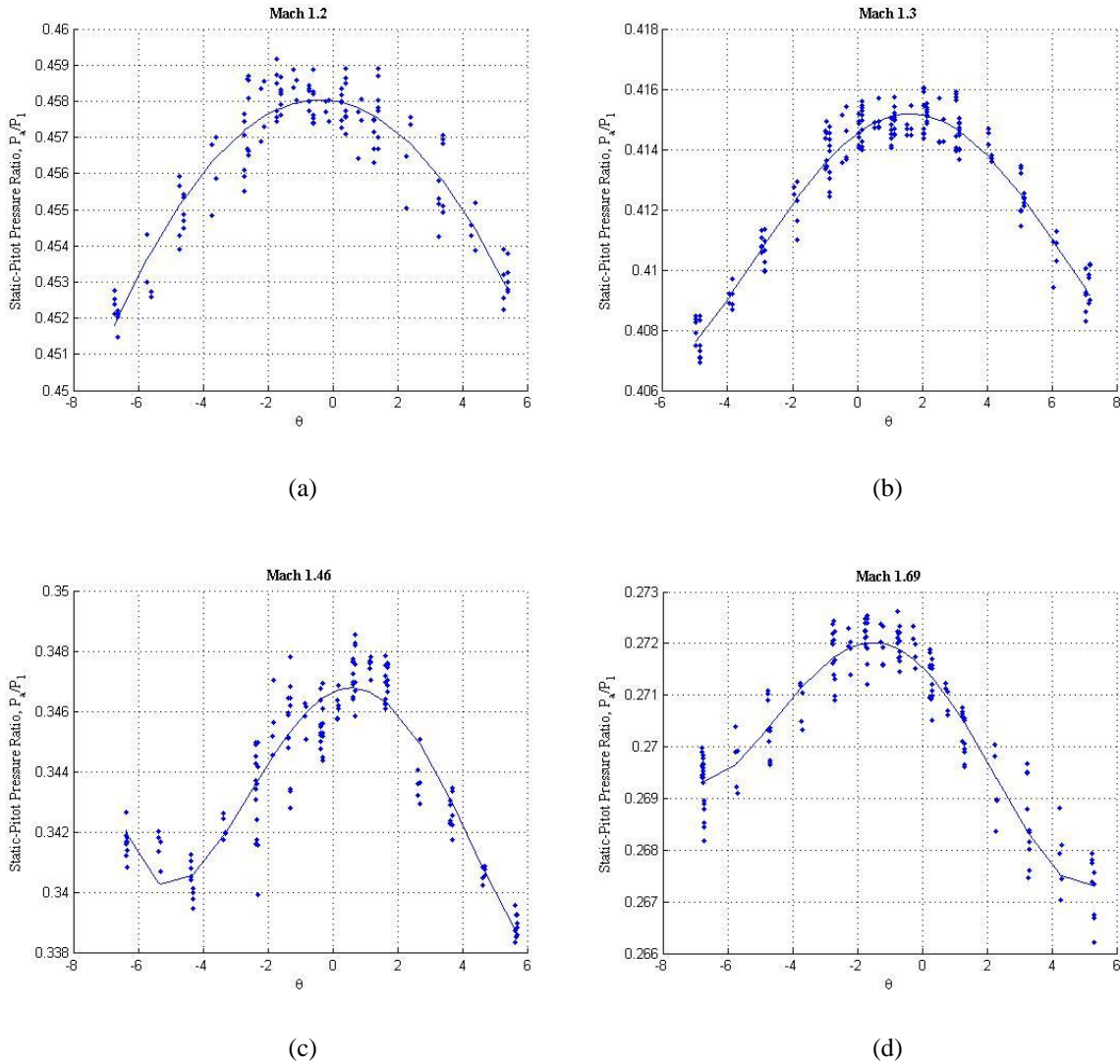


Figure 15. The static-pitot pressure ratio, $\frac{P_a}{P_1}$ is plotted as a function of the pitch angle, θ , which for this experimental setup included the angle of attack and the sideslip angle. The concave down trend is exhibited for all of the Mach test points, with θ ranging consistently between -8° to 8° . Also, the pressure ratio decreases with increasing Mach number. Like the previous plots of Mach 1.46 in Fig. 10c and 11c, its plot here (c) shows a distinctive upward trend in $\frac{P_a}{P_1}$ from about $\theta = -6.5^\circ$ to -4° , which is likely due to the inconsistent flow in the wind tunnel and the probe not being fixed in space. Further analysis will be conducted at this test point prior to flight testing of the CCIE.

concave down trend, with lower pressure ratio values at the extreme ends of the pitch angles. In addition, as the Mach number value rises, the static-pitot pressure ratio values decrease due to an increase in the total pressure, P_1 as well as a decrease in the average measured static pressures, P_a . The point of most interest from these plots will be the value of the static-pitot pressure when the pitch angle is 0° , i.e. $\left(\frac{P_a}{P_1}\right)_{\theta=0^\circ}$.¹³ It is the value at this point that is used to determine the estimated theoretical Mach number. To determine $\left(\frac{P_a}{P_1}\right)_{\theta=0^\circ}$, all static-pitot pressure ratio values between $\theta = -0.5^\circ$ to $\theta = 0.5^\circ$ were averaged at each Mach test point. The four resulting pressure ratio averages were plotted with the conical flow theory line as square markers in Fig. 16 for a visual comparison. Looking at the graph, the four wind tunnel test points at Mach 1.2, 1.3, 1.46, and 1.69 did fairly well in matching up with the conical flow theory trend. Table 4 displays a chart of both the theoretical and the wind tunnel static-pitot pressure ratio values at zero pitch angle at the four different Mach conditions. All the wind tunnel results fell within $\pm 2\%$ of the theoretical pressure ratio values. Since the wind tunnel results were close to theoretical values, the conical flow theory curve will be used to estimate the initial local Mach number in the RTF code. With the wind tunnel data analysis portion of the calibration completed, the next step is to perform uncertainty analysis on the calibrated results prior to implementing the calibration information into the in-flight RTF script.

III. Uncertainty Analysis

Most of the figures shown so far in this report have error bounds in place around their respective data points. Since this is typical of post-experimental data analysis, sample calculations will be placed in the Appendix as not to overwhelm this portion of the report with broad unnecessary details of how to calculate the error. Rather, the uncertainty analysis portion of the calibration involves finding the error associated with critical in-flight parameters, such as angle of attack, sideslip angle, Mach number, and dynamic pressure. Three different sources of error were obtained and they include uncertainty from the MSFC/ARF TWT's test runs, from the calibration graphs, and from error propagation due to the wind tunnel pressure transducers on the probe.

A. MSFC/ARF TWT Mach Number Uncertainty

As mentioned in the Introduction section of the report, the NASA MSFC/ARF TWT was recently upgraded and certification of the facility and its data measurement capabilities were detailed in a report entitled, "Calibration of Mach Number Set Points for the MSFC 14 x 14-Inch Trisonic Wind Tunnel," a joint paper between NASA and contractors, Jacobs Engineering, and Ducommun Miltec.¹⁵ One of the objectives for this particular Mach number calibration was to define the Mach centerline profiles for Mach numbers ranging from 0.2 to 2.5. A range of Mach

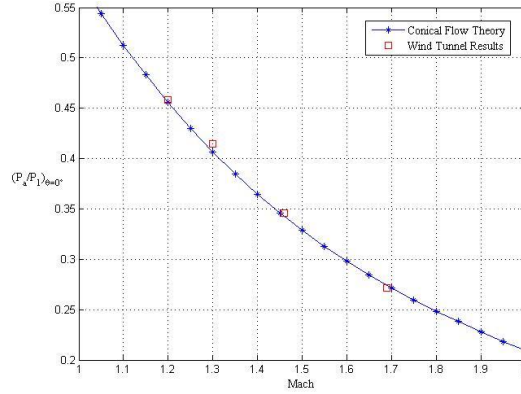
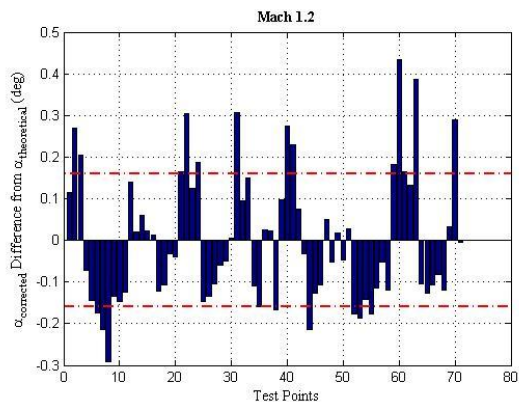


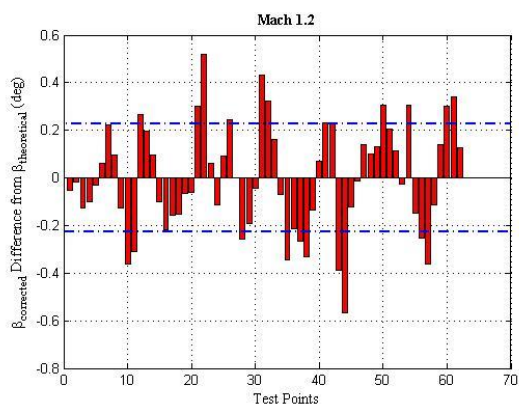
Figure 16. Theoretical and wind tunnel values of $\left(\frac{P_a}{P_1}\right)_{\theta=0^\circ}$ are plotted as a function of Mach number between Mach 1 and 2. The four test points at Mach 1.2, 1.3, 1.46, and 1.69 were particularly close to their theoretical values and their static-pitot pressure values at zero pitch angle decreased with increasing Mach number like the conical flow theory.

Table 4. The static-pitot pressure ratios for each of the Mach test points during the wind tunnel runs are displayed below along with their corresponding theoretical values from conical flow theory for comparison.

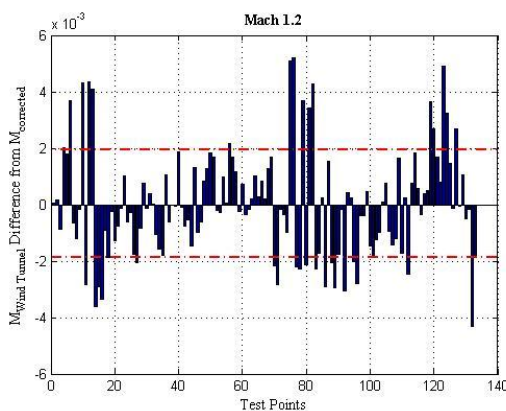
MACH	Theoretical $\left(\frac{P_a}{P_1}\right)_{\theta=0^\circ}$	Wind Tunnel $\left(\frac{P_a}{P_1}\right)_{\theta=0^\circ}$	Percentage Difference from Theoretical
1.20	0.4550	0.4579 ± 0.0008	+ 0.6374%
1.30	0.4067	0.4147 ± 0.0008	+ 1.9671%
1.46	0.3423	0.3457 ± 0.0008	+ 0.9932%
1.69	0.2739	0.2715 ± 0.0007	- 0.8762%



(a)



(b)



(c)

Figure 17. Mach 1.2's corrected angle of attack and sideslip angle difference from their theoretical best fit values are shown in (a) and (b). The Mach wind tunnel difference from the calibrated values is shown in (c). Standard deviation limits are shown as dotted horizontal lines.

reading uncertainty was produced for each Mach number to update the results of a previous calibration done in 1964. For the CCIE wind tunnel calibration, the Mach numbers of interest are 1.2, 1.3, 1.46, and 1.69. Based on the results of the report, the standard deviation for test points 1.2, 1.3, 1.46, and 1.69 were 0.0084, 0.011, 0.009, and 0.0095, respectively. These standard deviation values will be incorporated with the other Mach uncertainty values derived later on. Since only Mach number uncertainty was discussed in detail in the MSFC/ARF TWT paper, uncertainty for the other critical parameters had to be calculated through the calibration graphs and the hand calculations.

B. Uncertainty from the Calibration Graphs

Wind tunnel data, the resultant calibrated data, and for some variables, its theoretical lines of best fitted data, have quantitative differences with one another. In order to calculate the uncertainty here, error bar graphs were plotted depicting the differences between the calibrated data from the wind tunnel data. For angle of attack and sideslip angle, this difference was already addressed with the removal of the vertical misalignment angles. Instead for these two angular parameters, the error bar plots will show the difference between the corrected data and the theoretical values calculated based on the lines of best fit as shown in Fig. 9 with the Mach 1.2 case. These plots can be seen here in Fig. 17a and b for angle of attack and sideslip angle, respectively for Mach 1.2. Much of the difference between the corrected α and β values from their theoretical counterparts fell within one standard deviation of approximately 0.16 for the angle of attack case and 0.23 for the sideslip angle instance. The wind tunnel measurements of Mach number did fairly well when compared to its calibrated values as seen in Fig. 17c. Error differences were on the order of 10^{-3} with a standard deviation of approximately 0.002. These standard deviations were gathered for angle of attack, sideslip angle, and Mach number for the entire four Mach test runs of 1.2, 1.3, 1.46, and 1.69. Their quantities are displayed in Table 5 along with the other uncertainties. Similar figures for Mach 1.3, 1.46, and 1.69 were constructed like that of Mach 1.2's figures in Fig. 17 and can be referenced in the Appendix.

C. Uncertainty due to Error Propagation

This portion of the error analysis process was the most crucial during the calibration process and was performed along the way during the calibration process for each variable. The CCIE's pressure probes in the wind tunnel were rated with an uncertainty margin of ± 4 psf or about ± 0.0278 psi. Error from these probes of course would propagate throughout the calculation of

subsequent variables that are dependent upon them. With hundreds of data points for all of the four Mach test runs and dozens of variables to calculate for each data points, using MATLAB is the logical way to perform all the uncertainty analysis. To certify that the calculations are correct, hand calculations of error analysis were performed at a random data point for each variable. All of the data points had an error associated with it, but the most important critical in-flight parameters, like angle of attack, sideslip angle, Mach number, and dynamic pressure had their uncertainties averaged resulting in a single value for each Mach test run. Their respective uncertainty values are shown in Table 5. Sample calculations of the error analysis performed for these variables and other parameters are available in the Appendix for reference.

D. Combine the Uncertainty Results

Uncertainties from the wind tunnel, the calibration graphs, and due to error propagation for angle of attack, sideslip angle, Mach number, and dynamic pressure are all different. Since they were calculated independent of one another, the uncertainties could be combined using Eq. 27,

$$\delta(\alpha, \beta, M, Q_{bar}) = \sqrt{[(\alpha, \beta, M, Q_{bar})_{Wind\ Tunnel}]^2 + [(\alpha, \beta, M, Q_{bar})_{Calibration}]^2 + [(\alpha, \beta, M, Q_{bar})_{Error\ Propagation}]^2} \quad (27)$$

which is based on the root-sum squared method. The combined results are shown in Table 5 below along with the other calculated uncertainties for the other three sources for comparison. Mach number and dynamic pressure both had the least error. Angle of attack and sideslip angle had slightly larger error values, but were acceptable. If the vertical misalignment angle had not been removed, the error results would definitely have been much greater.

Table 5. The uncertainty values of angle of attack, α , sideslip angle, β , Mach number, and dynamic pressure, Q_{bar} for the wind tunnel, the calibration graphs, and the error propagation are displayed here along with their combined results for Mach 1.2, 1.3, 1.46, and 1.69.

		Mach 1.2	Mach 1.3	Mach 1.46	Mach 1.69
Wind Tunnel	α	-	-	-	-
	β	-	-	-	-
	Mach	0.0084	0.0110	0.0090	0.0095
	Q_{bar}	-	-	-	-
Calibration Graphs	α	0.15930	0.33860	0.23210	0.17710
	β	0.22770	0.28960	0.45720	0.27320
	Mach	0.00191	0.00388	0.00367	0.00340
	Q_{bar}	-	-	-	-
Error Propagation	α	0.29667	0.29695	0.31282	0.24138
	β	0.30081	0.31404	0.32548	0.24402
	Mach	0.00255	0.00274	0.00319	0.00353
	Q_{bar}	0.04778	0.05143	0.05851	0.07131
Combined Uncertainty Results	α	0.33673	0.45036	0.38952	0.29938
	β	0.37727	0.42719	0.56122	0.36631
	Mach	0.00898	0.01198	0.01023	0.01069
	Q_{bar}	0.04778	0.05143	0.05851	0.07131

IV. Create the In-Flight RTF Script

With the calibration completed and the uncertainty analysis taken care of, the results from the calibration could now be implemented into the in-flight RTF script to compute critical flight parameters during the experimental flight tests of the CCIE on the F-15B research aircraft. The script was written using MATLAB at first, but will later be converted into RTF with the aid of the computer engineers of NASA DFRC's Western Aeronautical Test Range (WATR), which provides useful resources for flight research operations and low earth-orbiting missions, such as mission control, communication, telemetry, and real-time data acquisition. Any MATLAB shortcuts, commands, or built-in functions had to be avoided in order for the script to be compatible with RTF.

The CCIE multi-hole pressure probe will measure pressures from five different ports, P_1 , P_2 , P_3 , P_4 , and P_5 as shown in Fig. 4. During an actual flight, the five measured pressures will be inputted into a function that will make an initial estimate of the Mach number based on the given flow conditions. The average probe static pressure, P_a will be calculated first in order to derive the static-pitot pressure ratio, $\frac{P_a}{P_1}$, which the Mach number is dependent upon. From Fig. 16, the conical flow theory trend line relates the static-pitot pressure ratio to Mach number in Eq. 28 as

$$M = -13.7965 \left(\frac{P_a}{P_1}\right)^3 + 21.1538 \left(\frac{P_a}{P_1}\right)^2 - 12.5144 \left(\frac{P_a}{P_1}\right) + 3.8167. \quad (28)$$

from which the estimated Mach number could be computed. The estimated Mach number and the five measured pressures would then be inputted into a different function that will then calculate the in-flight parameters of interest. The conical flow relationship between Mach number and the static-pitot pressure ratio shown in Eq. 28 is only valid for Mach numbers above 1.05. As a result, for estimated Mach numbers that are below 1.05, the function will tell

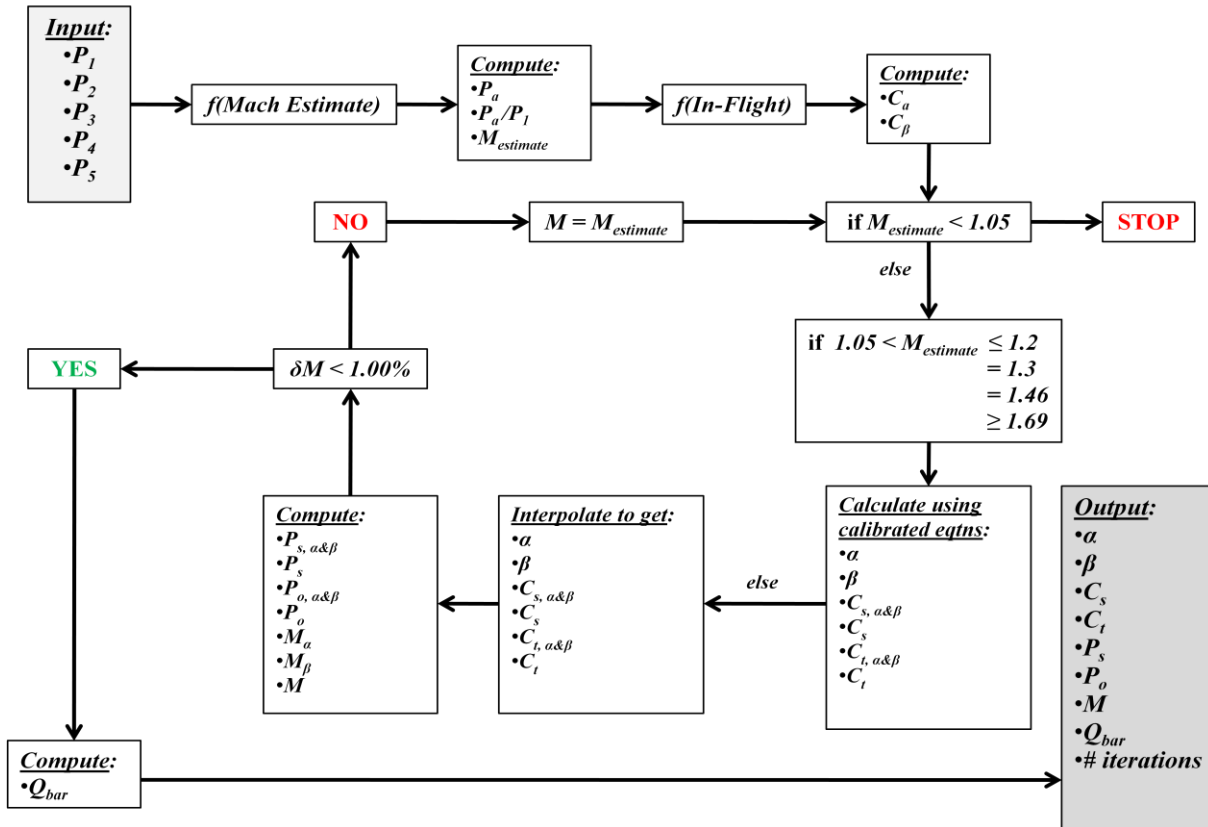


Figure 18. This flowchart shows a visual representation of how the in-flight RTF script would run on the mission control displays during a CCIE research experimental flight.

the code to stop running and not calculate anything. If the estimated Mach number is above 1.05 and on target at the CCIE Mach test points of 1.2, 1.3, 1.46, and 1.69, calibrated equations will be used to calculate variables, such as α , β , C_s , and C_t , otherwise other estimated Mach numbers will prompt the in-flight function to perform an interpolation to derive solutions for these variables. It should be noted that two values of C_t and C_s are calculated for the angle of attack and sideslip case, respectively. However, from Fig. 10 and 11 for the total pressure coefficient and Fig. 12 and 13 for the static pressure coefficient, the values of $C_{t\alpha}$ and $C_{t\beta}$ as well as $C_{s\alpha}$ and $C_{s\beta}$ are fairly close. As a result, the resulting averages of the angle of attack and sideslip values of both the total and static pressure coefficients will be sufficient for the values of C_t and C_s , respectively. Afterwards, the resultant variables α , β , C_s , and C_t would be used to calculate the static and total pressure, P_s and P_o , as well as the local Mach number. This Mach number should not be confused from the aircraft Mach number as it is based on the measured pressures of the CCIE, which is mounted underneath the aircraft. Again, averages between the α and β values of these variables are used to derive the final value. If the estimated Mach number and the newly derived in-flight Mach number have a difference of less than 1%, the function would output the critical in-flight parameters to the user in mission control and parameters include α , β , C_s , C_t , P_s , P_o , M , Q_{bar} , and the number of iterations it took to derive these solutions. If the estimated Mach number and the in-flight Mach number calculated have a difference greater than 1%, the in-flight Mach number becomes the new estimated Mach number and the in-flight function starts all over again until the convergence criteria is met.

V. Current Status of the Channeled Centerbody Inlet Experiment

The CCIE test fixture is currently undergoing preparation for research flights this upcoming summer of 2011. The aerodynamics group is performing the aerodynamic loads and CFD analysis with discussions underway to ensure the CCIE fixture's structural load integrity. The structures team will be involved in performing a ground vibrations test in order to guarantee that the CCIE test fixture has an adequate flutter clearance for flight safety. Instrumentation engineers are overseeing wiring and tubing connections and updating existing electrical design drawing to reflect the changes. In addition, operations will be involved in outlining flight test maneuvers, coordinating test activities, and monitoring any configuration changes. Also, WATR engineers will construct data displays in the mission control room for all organizations involved with the project and will include implementation the in-flight RTF script discussed earlier. Prior to the first flight, a Combined Systems Test (CST) will be performed to confirm the F-15 aircraft functionality by verifying the control room displays, RTF code, instrumentation, telemetry, and communication. The flights will gather information about the two CCIE configurations, one with the channeled centerbody and one with the smooth centerbody, and comparisons will be made between the two regarding mass flow, pressure recovery, and how well they perform with respect to the viscous CFD analysis. Post-flight data analysis will be conducted towards the end of the year.

VI. Conclusion

Enhanced supersonic and hypersonic cruise and acceleration will depend on an effective geometric inlet design capable of large air mass flow. The Channeled Centerbody Inlet Experiment research project done here at NASA Dryden Flight Research Center will prove crucial in this investigation. By testing out two different configurations with the channeled centerbody and the smooth centerbody, researchers hope to document the performance of each centerbody and compare the results of the flight test by validating the CFD findings. If the CCIE performs well and concurs with CFD results, the channeled centerbody concept could become a breakthrough for supersonic and hypersonic flight.

Wind tunnel testing of the CCIE multi-hole pressure probe yielded data results for four Mach conditions of 1.2, 1.3, 1.46, and 1.69 that needed to be calibrated in order to derive in-flight parameters. This conical probe calibration consisted of extensive steps in order to produce the desired calibrated results. By defining the probe orientation and coordinate system, calculations were much easier to determine the pressure coefficients, like C_{α} , C_{β} , C_t , and C_s . Next, the vertical misalignment angle, α_o and β_o were determined and removed from the data set so that the location where pressure coefficients, C_{α} and C_{β} remain independent of roll angle at zero degrees angle of attack or sideslip in order to reflect more like the theoretical case. Afterwards, angle of attack, sideslip angle, total and static pressure coefficients had their equations derived to reflect their best fit trends. Flow properties were then computed to reflect the calibrated case and static-pitot pressure ratio trends were created to determine how well the wind tunnel results fit with the conical flow theory. The uncertainty analysis was then performed and consisted of calculating error from three different sources, which include the wind tunnel, the calibration graphs, and error propagation with the aid of MATLAB and self-check. The uncertainties were then combined and with the uncertainties within reasonable

limits, the calibrated results were then assimilated into the in-flight RTF script, which will calculate critical in-flight parameters, such as angle of attack, sideslip angle, dynamic pressure, and Mach number.

With the CCIE in preparation for its research flights, there is much anticipation of what the flight results may turn out like. Results from this research project could contribute to a tremendous amount of new information on how to enrich supersonic and hypersonic flight. As the world heads deeper into the 21st century, technology will only continue to advance and improve, including the world of aeronautics. NASA Dryden Flight Research Center has been at the forefront of aeronautics research for over 50 years and it will continue to be a place of innovation for future enhanced aircraft performance.

Appendix

A. Additional Calibration Figures

1) Vertical Misalignment

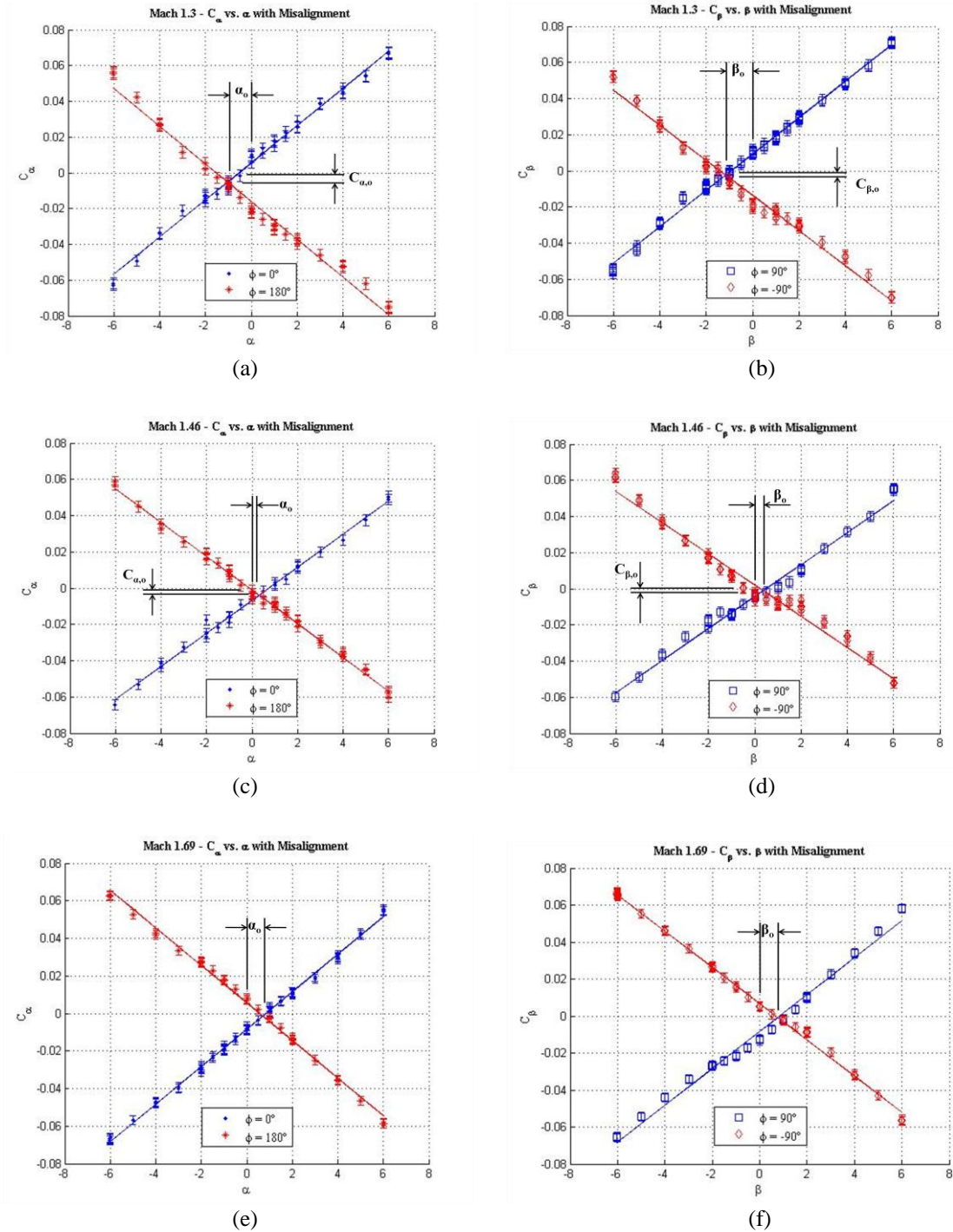


Figure 19. Analogous to Fig. 4 with the Mach 1.2 case, the vertical misalignments are shown here for both angle of attack and sideslip for Mach 1.3 (a & b), Mach 1.46 (c & d), and Mach 1.69's α and β -pitch coefficient offsets, C_{α_0} and C_{β_0} are very small and cannot be shown. The sizes of the misalignments, α_o and β_o can be compared to that of Table 1.

2) Vertical Misalignment Removed

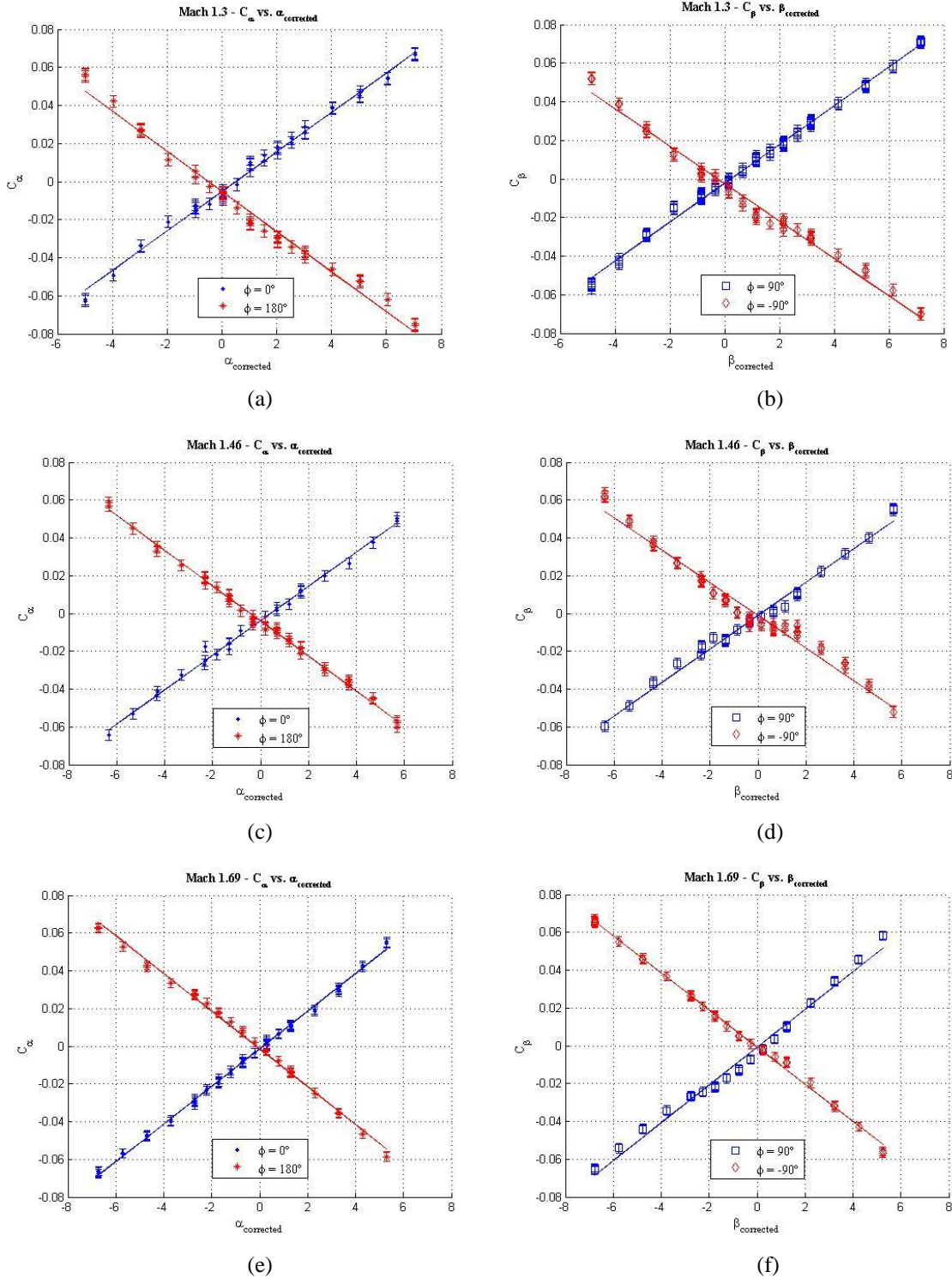


Figure 20. Like the Mach 1.2 example shown in Fig. 5, the vertical misalignment angles are removed here for both the angle of attack and sideslip angle instances for Mach 1.3 (a & b), Mach 1.46 (c & d), and Mach 1.60 (e & f).

3) Original α and β Comparison to Corrected α and β

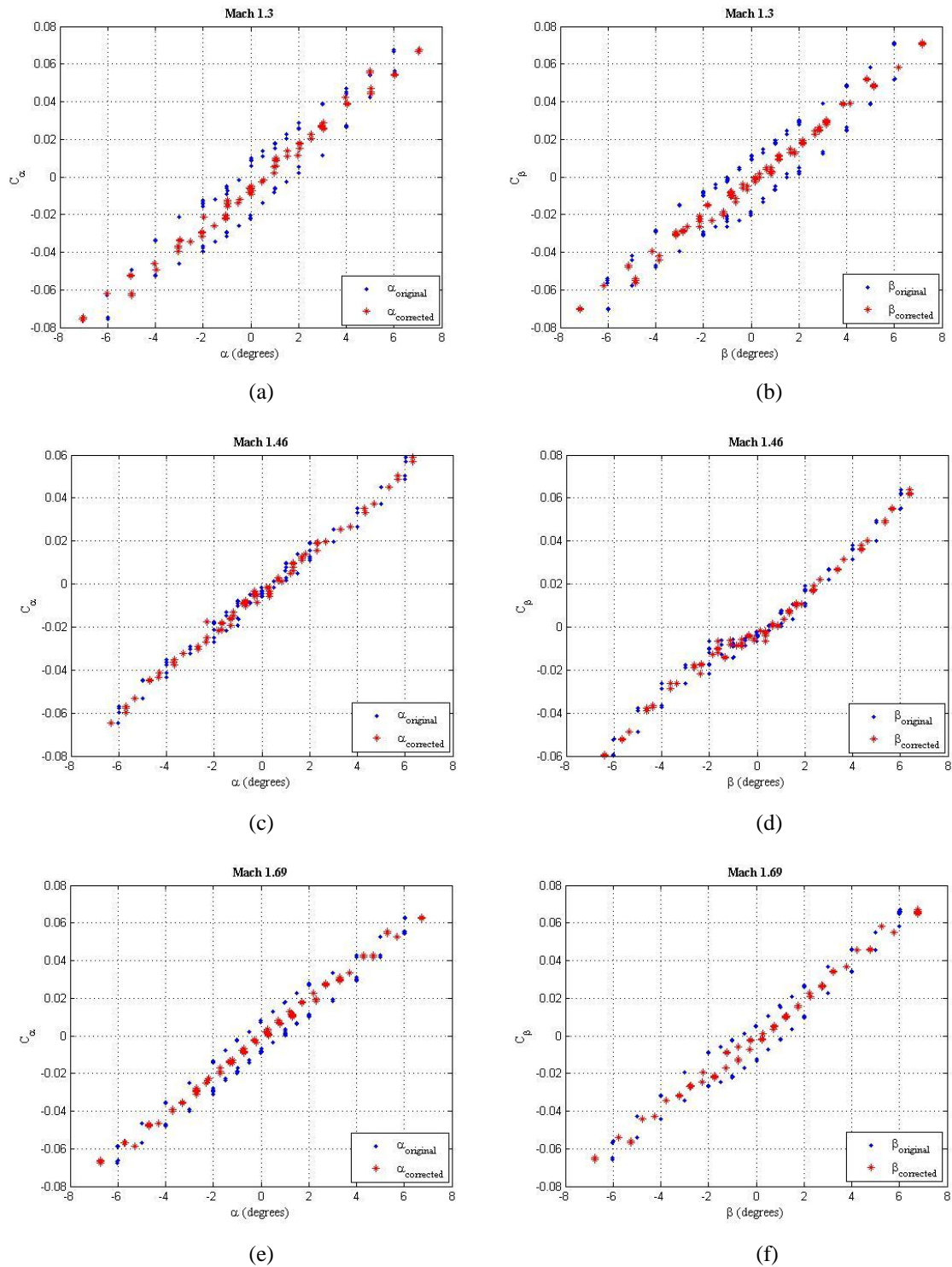


Figure 21. $\alpha_{original}$ and $\beta_{original}$ are plotted with their respective corrected values for Mach 1.3 (a & b), Mach 1.46 (c & d), and Mach 1.69 (e & f), similar to the plots of Mach 1.2 in Fig. 6. The separation between the original and corrected data points represent the vertical misalignment, with Mach 1.46 having the least bias and Mach 1.3 having the most. However, Mach 1.46's trend is not as linear as the others.

4) $\alpha_{\text{corrected}}$ and $\beta_{\text{corrected}}$ Best Fit Trends

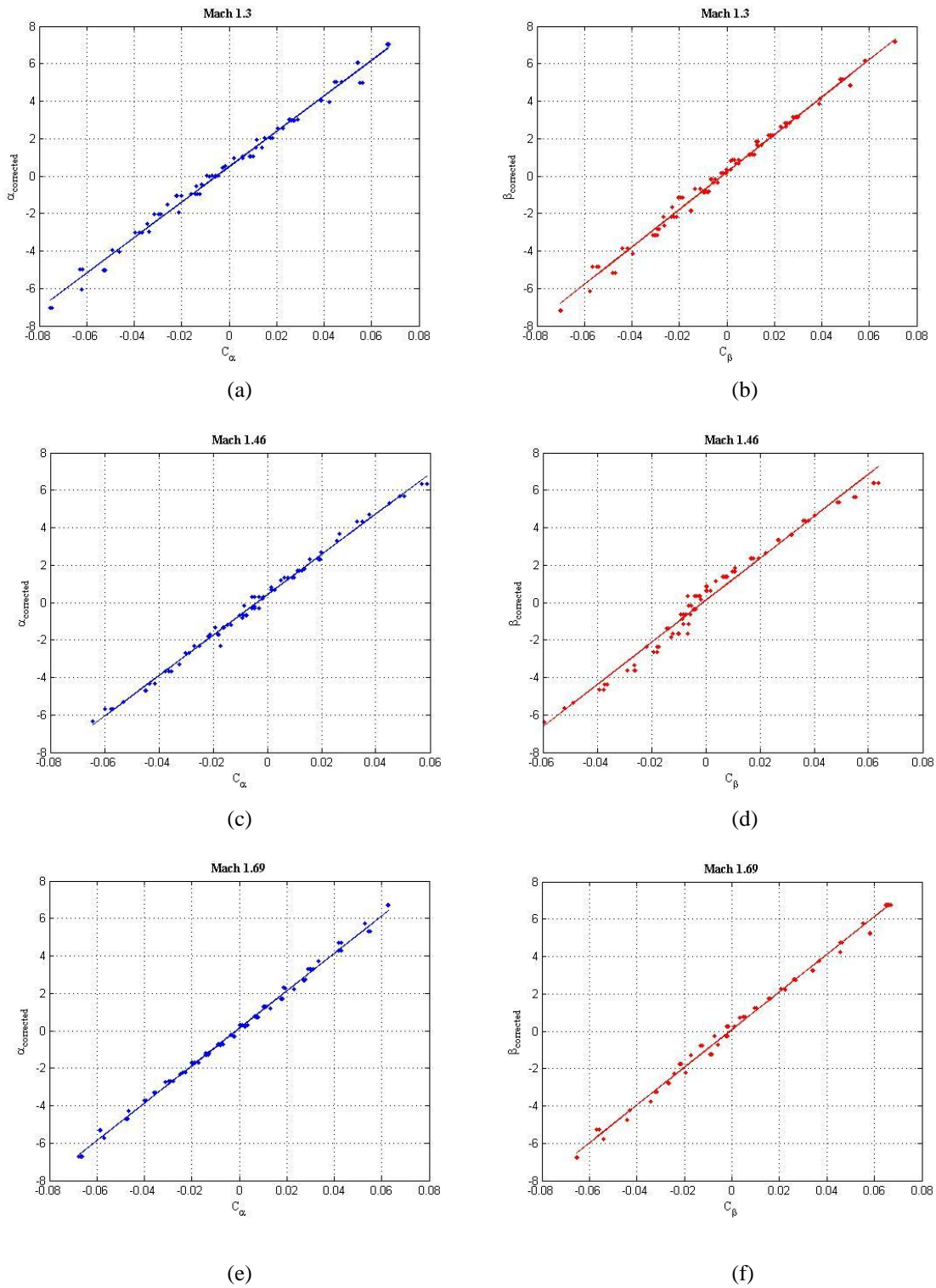
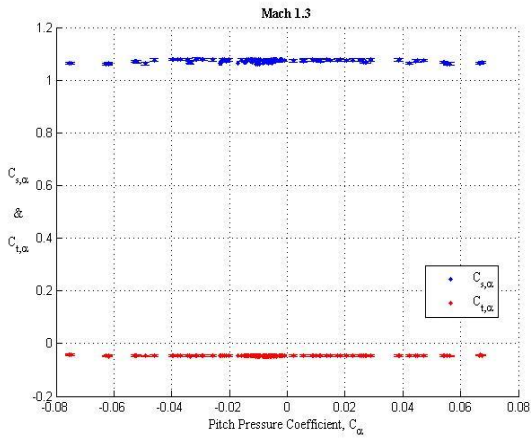
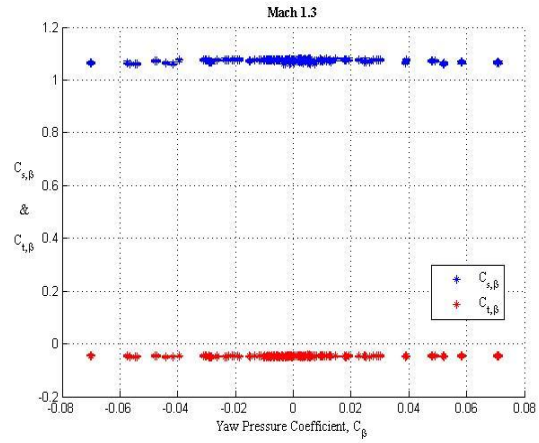


Figure 22. The $\alpha_{\text{corrected}}$ and $\beta_{\text{corrected}}$ best fit trends, which represents the theoretical linear relationship of angle of attack and sideslip angle with their respective pressure coefficients, are shown here for Mach 1.3 (a & b), Mach 1.46 (c & d), and Mach 1.69 (e & f). Comparing it to Mach 1.2's plots in Fig. 7, Mach 1.2 and 1.69 fit fairly well, while the sideslip case for Mach 1.46 seemed to exhibit a higher-order behavior.

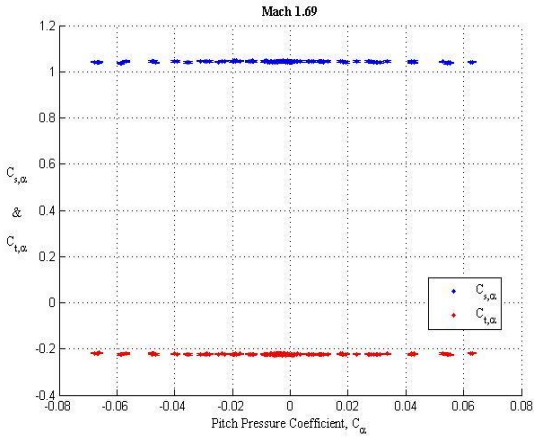
5) Static and Total Pressure Coefficient Comparison



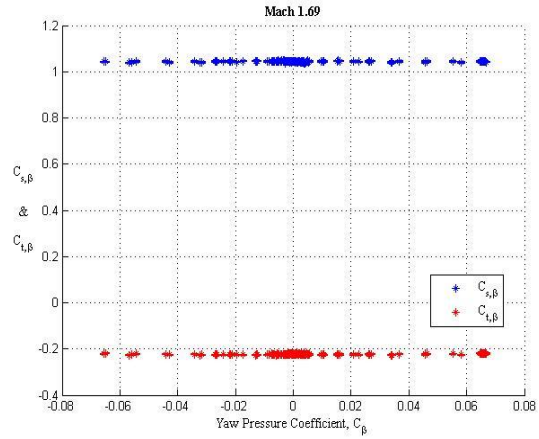
(a)



(b)



(c)



(d)

Figure 23. Like the Mach 1.2 and 1.46 plots shown in Fig.12, the static and total pressure coefficient values for both the angle of attack and sideslip angle cases are plotted for the Mach 1.3 (a & b) and Mach 1.69 (c & d) simultaneously. Notice how the total pressure coefficient values of $C_{t,\alpha}$ and $C_{t,\beta}$ linger around zero and the static pressure coefficient values of $C_{s,\alpha}$ and $C_{s,\beta}$ hover around one.

B. Additional Calibration Uncertainty Graphs

1) Corrected Angle of Attack Difference From Theoretical

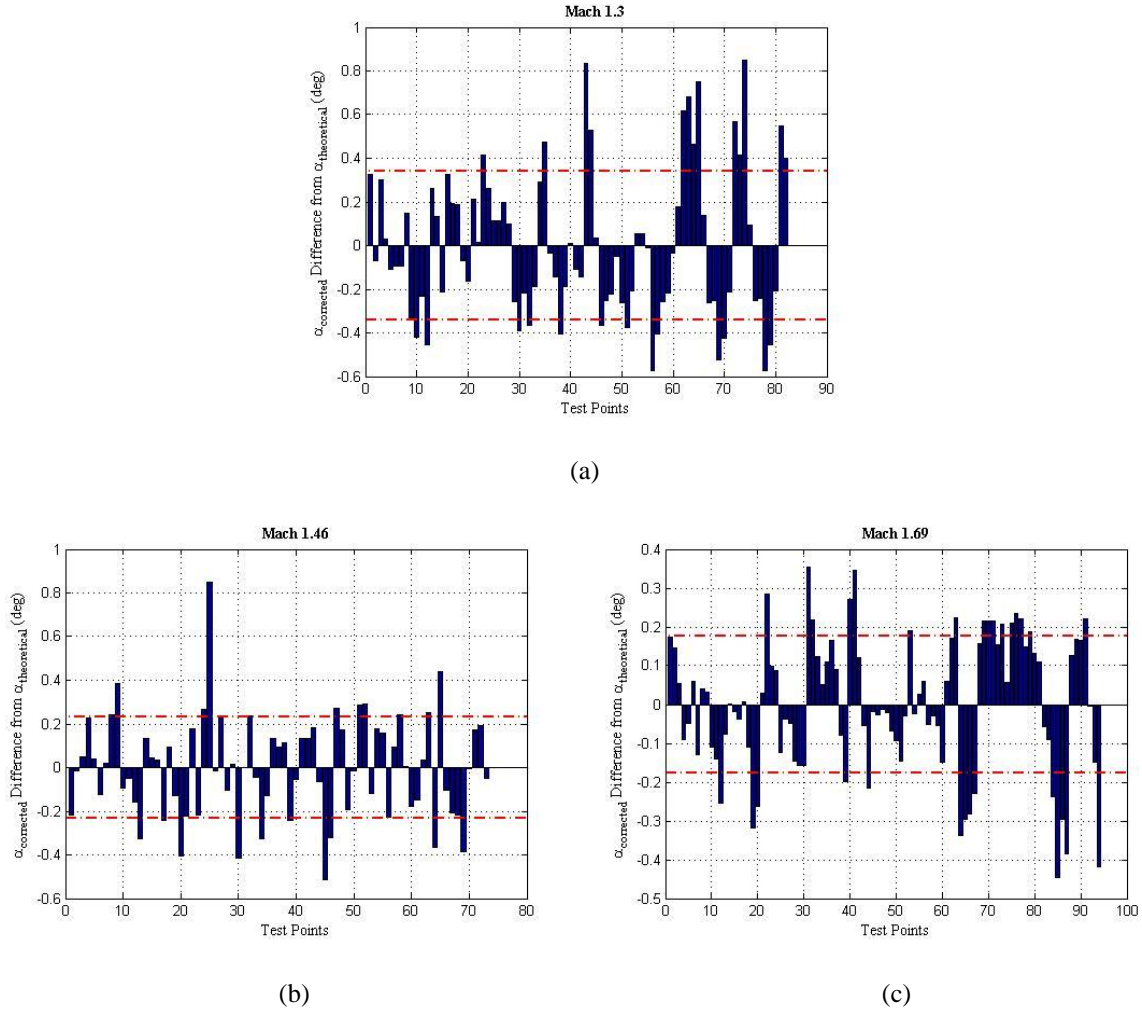


Figure 24. Similar to Mach 1.2's $\alpha_{corrected}$ difference from theoretical graph in Fig. 15a, the calibration error bar graphs for the angle of attack case are shown here for Mach 1.3 (a), Mach 1.46 (b), and Mach 1.69 (c). Each Mach test run has differing number of test points. As seen from these figures, much of the data results fell within the standard deviation dashed lines. The standard deviation corresponding to these error bar graphs could be viewed in Table 5 under the calibrations graphs section.

2) Corrected Sideslip Angle Difference From Theoretical

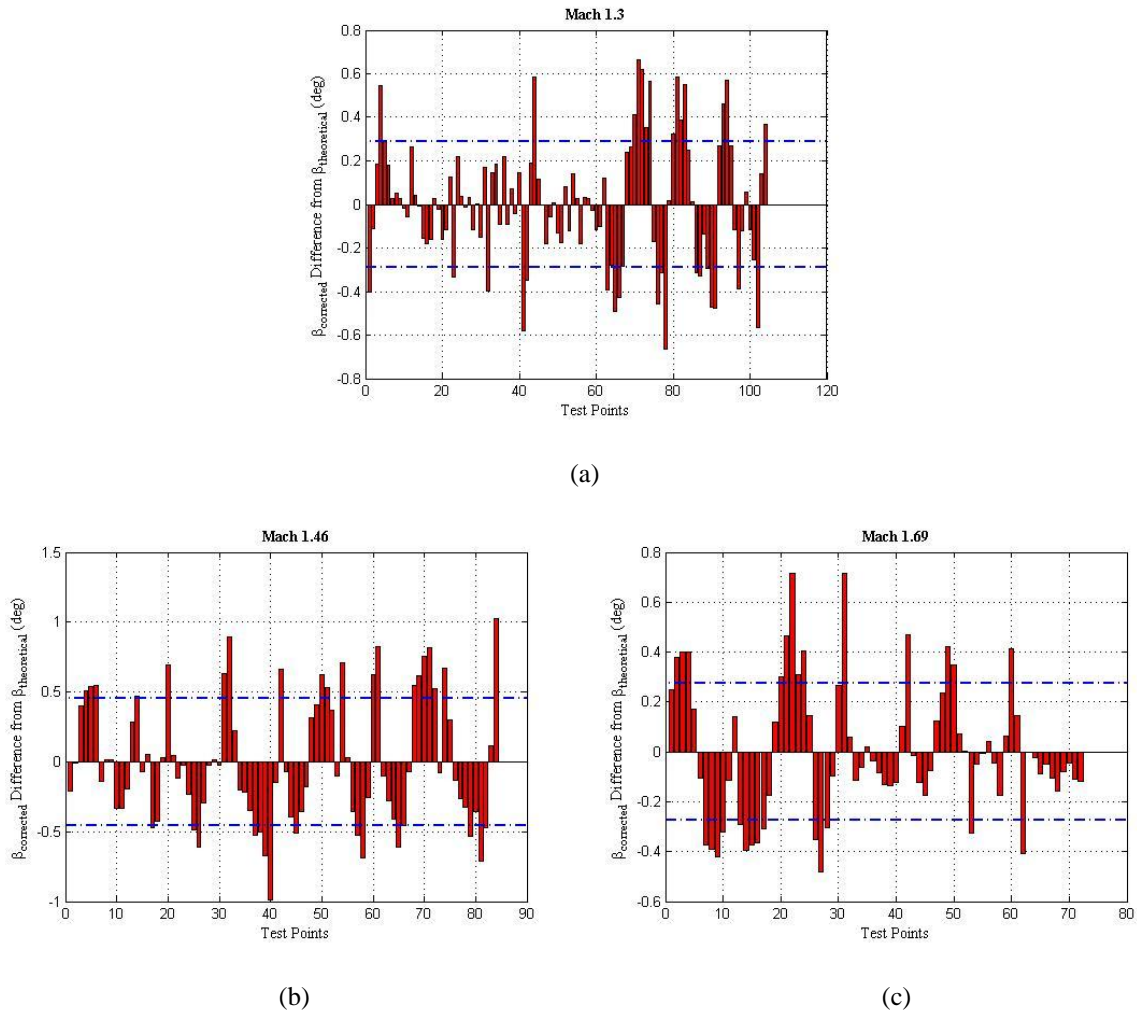
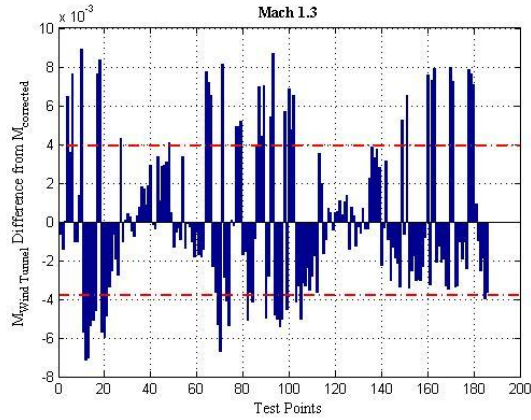
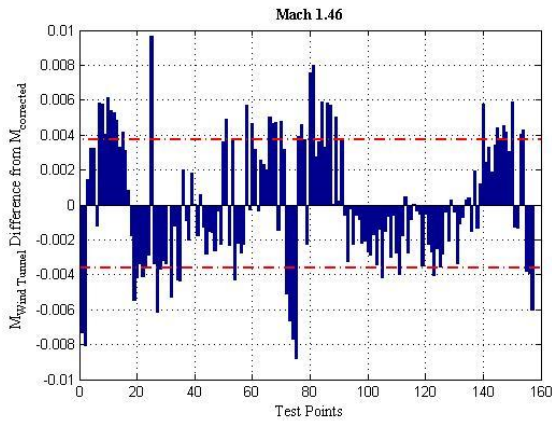


Figure 25. Mach 1.2's corrected sideslip error difference from its theoretical counterpart was shown in Fig. 15b and the case for Mach 1.3 (a), Mach 1.46 (b), and Mach 1.69 (c) are shown here. Mach 1.46 had the largest difference of all the Mach test points and from Fig. 20d, its corrected data points were a bit off from the linear trend line, which explained why it had a wider standard deviation margin.

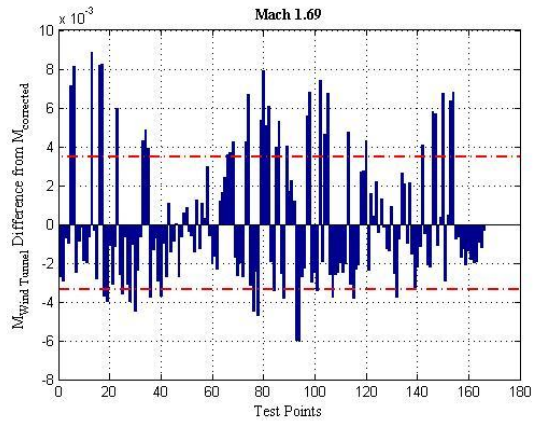
3) Wind Tunnel Mach Number Difference From Corrected



(a)



(b)



(c)

Figure 26. Like the error bar difference for Mach 1.2 in Fig. 15c, the error between the wind tunnel Mach number and the corrected Mach number for Mach 1.3 (a), Mach 1.46 (b), and Mach 1.69 (c) have small standard deviation values with all of them having deviations of less than 0.5%.

C. Sample Error Calculations

The method that was used to calculate the uncertainties for many of the variables during the calibration are shown here. This process was both done in MATLAB for the many test points and by hand for a random test point to verify MATLAB's accuracy. Results for critical parameters like α , β , M , and Q_{bar} were shown in Table 5.

- 1) Error Process for Calculating P_a , C_α , C_β , C_t , C_s , α_o , C_{α_o} , β_o , C_{β_o} and $\frac{P_a}{P_1}$

The trisonic wind tunnel pressure transducers' uncertainty on the CCIE pressure probes is rated at about $dp = \pm 0.0278$ psi. Using P_a as an example from Eq. 1, the error for P_a should be calculated as follows:

$$\delta(P_2) = \left(\frac{1}{4} [(P_2 + dp) + P_3 + P_4 + P_5] \right) - P_a$$

$$\delta(P_3) = \left(\frac{1}{4} [P_2 + (P_3 + dp) + P_4 + P_5] \right) - P_a$$

$$\delta(P_4) = \left(\frac{1}{4} [P_2 + P_3 + (P_4 + dp) + P_5] \right) - P_a$$

$$\delta(P_5) = \left(\frac{1}{4} [P_2 + P_3 + P_4 + (P_5 + dp)] \right) - P_a$$

$$\boxed{\delta(P_a) = \left[(\delta(P_2))^2 + (\delta(P_3))^2 + (\delta(P_4))^2 + (\delta(P_5))^2 \right]^{\frac{1}{2}}} \quad (29)$$

The remaining variables could be calculated in a similar manner.

- 2) Error Process for Calculating Mach Number

Based on Eq. 23 and 24, the error in the calibrated Mach number for the angle of attack and sideslip angle case could be calculated as,

$$\frac{\partial M}{\partial P_o} = \frac{\sqrt{2} \left(\frac{P_s}{P_o} \right)^{\frac{1}{\gamma}}}{\left[\left(P_o - P_s \left(\frac{P_s}{P_o} \right)^{\frac{1}{\gamma}} \right) \left(\frac{P_s}{P_o} \right)^{\frac{1}{\gamma}} \right]^{\frac{1}{2}}}$$

$$\frac{\partial M}{\partial P_s} = \frac{-\sqrt{2} P_o \left(\frac{P_s}{P_o} \right)^{\frac{1}{\gamma}}}{\left[- \left(\frac{P_s}{P_o} \right)^{\frac{1}{\gamma}} \left(P_s \left(\frac{P_s}{P_o} \right)^{\frac{1}{\gamma}} - P_o \right) \right]^{\frac{1}{2}}}$$

$$\boxed{\delta M = \left[\left(\frac{\partial M}{\partial P_o} \cdot dP_o \right)^2 + \left(\frac{\partial M}{\partial P_s} \cdot dP_s \right)^2 \right]^{\frac{1}{2}}} \quad (30)$$

3) Error Process for Calculating $Q_{\text{bar-true}}$

Based on Eq. 25 and 26, the error in the calibrated dynamic pressure can be calculated as,

$$\frac{\partial \bar{q}_{\text{true}}}{\partial P_s} = \frac{1}{2} \gamma M^2$$

$$\frac{\partial \bar{q}_{\text{true}}}{\partial M} = \gamma M^2$$

$$\delta(\bar{q}_{\text{true}}) = \left[\left(\frac{\partial \bar{q}_{\text{true}}}{\partial P_s} \cdot dP_s \right)^2 + \left(\frac{\partial \bar{q}_{\text{true}}}{\partial M} \cdot dM \right)^2 \right]^{\frac{1}{2}} \quad (31)$$

D. MATLAB In-Flight RTF Script

1) Function to Estimate Initial Mach Number (est_mach.m)

```
function [est_mach] = est_mach(P1,P2,P3,P4,P5)
%
% EST_MACH - Calculate the initial estimate of the Mach number based on
% the conical static-pitot pressure ratio vs. Mach relation
% from the in-flight measured pressures obtained.
%
% EST_MACH(P1,P2,P3,P4,P5) - Input in-flight measured pressures
% results to calculate the static-pitot pressure ratio, which in turn
% outputs an initial estimate of Mach number. The initial guess will
% then be inputted into the INFLIGHT.m function to calculate the
% remainder parameters of interest and the corrected Mach number based
% on the calibration tables.
%
% By: Samson S. Truong
% Edited by: Mike Frederick
%=====
% Nomenclature
%
% est_mach - Initial Estimate of Mach Number
% Pratio - Static-Pitot Pressure Ratio (Pa/P1 or Pa/Pt2)
% P1 - Measured Total Pressure (psi)
% P2,P3,P4,P5 - Measured Static Pressures (psi)
% Pa - Average Measured Static Pressure (psi)
%=====
%-----
% Calculate Average Static Pressure, Pa
%-----
Pa = 0.25*(P2+P3+P4+P5);
%-----
% Calculate Static-Pitot Pressure Ratio, Pa/P1 (or) Pa/Pt2
%-----
Pratio = Pa./P1;
```

```

%-----
% Calculate Estimated Mach
%-----
est_mach = -13.7965.*Pratio.^3 + 21.1538.*Pratio.^2 - 12.5144.*Pratio + 3.8167;

%-----
% Call out In-Flight Function (inflight.m)
%-----
[iter,alpha,beta,Ca,Cb,Cs,Ct,Ps,Pt,MACH,dm,QBAR] = inflight(P1,P2,P3,P4,P5,est_mach)

```

2) Function to Calculate Critical In-Flight Parameters (inflight.m)

```

function [iter,alpha,beta,Ca,Cb,Cs,Ct,Ps,Pt,MACH,dm,QBAR] = inflight(P1,P2,P3,P4,P5,est_mach)
%
% INFLIGHT - Calculate flight parameters of interests using in-flight
%           measured pressures and interpolating results in-between
%           calibrated test points
%
% INFLIGHT(P1,P2,P3,P4,P5,mach) - Input in-flight measured pressures &
% initial Mach number guess, to output angle of attack, sideslip
% angle, MACH, and other significant flight data parameters using
% interpolation of the test points of interests at Machs 1.2, 1.3,
% 1.46, & 1.69.
%
% By: Samson S. Truong
% Edited by: Mike Frederick
%=====
%           Nomenclature
%
% alpha      - Angle of Attack (deg)
% beta       - Sideslip Angle (deg)
% Ca         - Pressure Coefficient w/respect to Angle of Attack
% Cb         - Pressure Coefficient w/respect to Sideslip Angle
% Cs         - Average Static Pressure Coefficient
% Csa        - Static Pressure Coefficient w/respect to Angle of Attack
% Csb        - Static Pressure Coefficient w/respect to Sideslip Angle
% Ct         - Average Total Pressure Coefficient
% Cta        - Total Pressure Coefficient w/respect to Angle of Attack
% Ctb        - Total Pressure Coefficient w/respect to Sideslip Angle
% dm         - Change in Mach Number
% est_mach   - Initial Estimate of Mach Number
% gamma      - Ratio of Specific Heats
% iter       - # of Iterations for Solution Convergence
% MACH       - Average Mach Number
% macha      - Mach Number w/respect to Angle of Attack
% machb      - Mach Number w/respect to Sideslip Angle
% P1         - Measured Total Pressure (psi)
% P2,P3,P4,P5 - Measured Static Pressures (psi)
% Pa         - Average Measured Static Pressure (psi)
% Ps         - Average In-Flight Static Pressure (psi)
% Psa        - In-Flight Static Pressure w/respect to Angle of Attack (psi)
% Psb        - In-Flight Static Pressure w/respect to Sideslip Angle (psi)
% Pt         - Average In-Flight Total Pressure (psi)
% Pta        - In-Flight Total Pressure w/respect to Angle of Attack (psi)

```

```

% Ptb      - In-Flight Total Pressure w/respect to Sideslip Angle (psi)
% pQBAR    - Pseudo-Dynamic Pressure (psi)
% QBAR     - Average In-Flight Dynamic Pressure (psf)
% QBARa    - In-Flight Dynamic Pressure w/respect to Angle of Attack (psf)
% QBARb    - In-Flight Dynamic Pressure w/respect to Sideslip Angle (psf)
%
%=====

%Ratio of Specific Heat Coefficient
gamma = 1.4;

%Calculate Average Static Pressure, Pa
Pa = 0.25*(P2+P3+P4+P5);

%Calculate Pseudo Dynamic Pressure, pQBAR
pQBAR = P1 - Pa;

%Pressure Coefficient w/respect to Angle of Attack, Ca:
Ca = (P3-P5)/(P1-Pa);

%Pressure Coefficient w/respect to Sideslip Angle, Cb:
Cb = (P4-P2)/(P1-Pa);

%% Begin While Loop

i = 1;
stop = 0;

if est_mach < 1.05
    disp('Estimated Mach Value is below 1.05. Code Terminated.')
end

while stop == 0
    if est_mach < 1.05
        break
    end
%-----
%Calculate solutions from calibration tables.
%-----
% l = low end & h = high end

if est_mach <= 1.20
    alpha1_2(i) = 89.1385*Ca + 0.7089;
    beta1_2(i) = 90.4277*Cb + 0.28410;
    Csa1_2(i) = -2.6378*Ca^2 - 0.043026*Ca + 1.0786;
    Csb1_2(i) = -2.3004*Cb^2 - 0.023978*Cb + 1.0776;
    Cta1_2(i) = 7.9419e-04*Ca - 0.015497;
    Ctb1_2(i) = -0.0010123*Cb - 0.015517;
elseif (est_mach > 1.20) && (est_mach < 1.30)
    alphas(i) = 89.1385*Ca + 0.7089;
    alphah(i) = 94.6015*Ca + 0.5037;
    betal(i) = 90.4277*Cb + 0.28410;
    betah(i) = 100.0237*Cb + 0.2179;
    Csal(i) = -2.6378*Ca^2 - 0.043026*Ca + 1.0786;
    Cсах(i) = -2.7522*Ca^2 - 0.021851*Ca + 1.0765;
    Csbl(i) = -2.3004*Cb^2 - 0.023978*Cb + 1.0776;

```

```

Csbh(i) = -2.7696*Cb^2 + 0.023859*Cb + 1.0756;
Ctal(i) = 7.9419e-04*Ca - 0.015497;
Ctah(i) = 0.43365*Ca^2 - 1.2153e-04*Ca - 0.046727;
Ctbl(i) = -0.0010123*Cb - 0.015517;
Ctbh(i) = 0.38196*Cb^2 + 0.0045245*Cb - 0.047481;
elseif est_mach == 1.30
alpha1_3(i) = 94.6015*Ca + 0.5037;
beta1_3(i) = 100.0237*Cb + 0.2179;
Csa1_3(i) = -2.7522*Ca^2 - 0.021851*Ca + 1.0765;
Csb1_3(i) = -2.7696*Cb^2 + 0.023859*Cb + 1.0756;
Cta1_3(i) = 0.43365*Ca^2 - 1.2153e-04*Ca - 0.046727;
Ctb1_3(i) = 0.38196*Cb^2 + 0.0045245*Cb - 0.047481;
elseif (est_mach > 1.3) && (est_mach < 1.46)
alpha(i) = 94.6015*Ca + 0.5037;
alphah(i) = 108.0175*Ca + 0.4175;
beta(i) = 100.0237*Cb + 0.2179;
betah(i) = 112.3877*Cb + 0.1192;
Csal(i) = -2.7522*Ca^2 - 0.021851*Ca + 1.0765;
Csa(i) = 8.5362*Ca^3 - 3.3971*Ca^2 - 0.038168*Ca + 1.0618;
Csb(i) = -2.7696*Cb^2 + 0.023859*Cb + 1.0756;
Csbh(i) = 17.772*Cb^3 - 3.2717*Cb^2 - 0.021265*Cb + 1.0618;
Ctal(i) = 0.43365*Ca^2 - 1.2153e-04*Ca - 0.046727;
Ctah(i) = 0.0086243*Ca - 0.090352;
Ctbl(i) = 0.38196*Cb^2 + 0.0045245*Cb - 0.047481;
Ctbh(i) = 0.024073*Cb - 0.090279;
elseif est_mach == 1.46;
alpha1_46(i) = 108.0175*Ca + 0.4175;
beta1_46(i) = 112.3877*Cb + 0.1192;
Csa1_46(i) = 8.5362*Ca^3 - 3.3971*Ca^2 - 0.038168*Ca + 1.0618;
Csb1_46(i) = 17.772*Cb^3 - 3.2717*Cb^2 - 0.021265*Cb + 1.0618;
Cta1_46(i) = 0.0086243*Ca - 0.090352;
Ctb1_46(i) = 0.024073*Cb - 0.090279;
elseif (est_mach > 1.46) && (est_mach < 1.69)
alpha(i) = 108.0175*Ca + 0.4175;
alphah(i) = 99.9231*Ca + 0.1318;
beta(i) = 112.3877*Cb + 0.1192;
betah(i) = 100.8961*Cb + 0.0871;
Csal(i) = 8.5362*Ca^3 - 3.3971*Ca^2 - 0.038168*Ca + 1.0618;
Csa(i) = -1.3094*Ca^2 - 0.024019*Ca + 1.045;
Csb(i) = 17.772*Cb^3 - 3.2717*Cb^2 - 0.021265*Cb + 1.0618;
Csbh(i) = -0.78067*Cb^2 + 0.0078296*Cb + 1.0452;
Ctal(i) = 0.0086243*Ca - 0.090352;
Ctah(i) = 0.72013*Ca^2 - 0.010757*Ca - 0.22335;
Ctbl(i) = 0.024073*Cb - 0.090279;
Ctbh(i) = 0.96616*Cb^2 + 0.012028*Cb - 0.22493;
elseif est_mach >= 1.69
alpha1_69(i) = 99.9231*Ca + 0.1318;
beta1_69(i) = 100.8961*Cb + 0.0871;
Csa1_69(i) = -1.3094*Ca^2 - 0.024019*Ca + 1.045;
Csb1_69(i) = -0.78067*Cb^2 + 0.0078296*Cb + 1.0452;
Cta1_69(i) = 0.72013*Ca^2 - 0.010757*Ca - 0.22335;
Ctb1_69(i) = 0.96616*Cb^2 + 0.012028*Cb - 0.22493;
end

```

```

%-----
% Interpolate solutions for alpha, beta, Csa, Csb, Cta, & Ctb
% (if between calibrated test points)
%-----
if est_mach <= 1.20
    alpha(i) = alpha1_2(i);
    beta(i) = beta1_2(i);
    Csa(i) = Csa1_2(i);
    Csb(i) = Csb1_2(i);
    Cs(i) = 0.5*(Csa(i) + Csb(i));
    Cta(i) = Cta1_2(i);
    Ctb(i) = Ctb1_2(i);
    Ct(i) = 0.5*(Cta(i) + Ctb(i));
elseif (est_mach > 1.20) && (est_mach < 1.30)
    Mh = 1.3;
    Ml = 1.2;
    alpha(i) = alphas(i) + ((est_mach - Ml)/(Mh - Ml))*(alphah(i) - alphas(i));
    beta(i) = betas(i) + ((est_mach - Ml)/(Mh - Ml))*(betah(i) - betas(i));
    Csa(i) = Csal(i) + ((est_mach - Ml)/(Mh - Ml))*(Csah(i) - Csal(i));
    Csb(i) = Csbl(i) + ((est_mach - Ml)/(Mh - Ml))*(Csbh(i) - Csbl(i));
    Cs(i) = 0.5*(Csa(i) + Csb(i));
    Cta(i) = Ctal(i) + ((est_mach - Ml)/(Mh - Ml))*(Ctah(i) - Ctal(i));
    Ctb(i) = Ctbl(i) + ((est_mach - Ml)/(Mh - Ml))*(Ctbh(i) - Ctbl(i));
    Ct(i) = 0.5*(Cta(i) + Ctb(i));
elseif est_mach == 1.30
    alpha(i) = alpha1_3(i);
    beta(i) = beta1_3(i);
    Csa(i) = Csa1_3(i);
    Csb(i) = Csb1_3(i);
    Cs(i) = 0.5*(Csa(i) + Csb(i));
    Cta(i) = Cta1_3(i);
    Ctb(i) = Ctb1_3(i);
    Ct(i) = 0.5*(Cta(i) + Ctb(i));
elseif (est_mach > 1.3) && (est_mach < 1.46)
    Mh = 1.46;
    Ml = 1.3;
    alpha(i) = alphas(i) + ((est_mach - Ml)/(Mh - Ml))*(alphah(i) - alphas(i));
    beta(i) = betas(i) + ((est_mach - Ml)/(Mh - Ml))*(betah(i) - betas(i));
    Csa(i) = Csal(i) + ((est_mach - Ml)/(Mh - Ml))*(Csah(i) - Csal(i));
    Csb(i) = Csbl(i) + ((est_mach - Ml)/(Mh - Ml))*(Csbh(i) - Csbl(i));
    Cs(i) = 0.5*(Csa(i) + Csb(i));
    Cta(i) = Ctal(i) + ((est_mach - Ml)/(Mh - Ml))*(Ctah(i) - Ctal(i));
    Ctb(i) = Ctbl(i) + ((est_mach - Ml)/(Mh - Ml))*(Ctbh(i) - Ctbl(i));
    Ct(i) = 0.5*(Cta(i) + Ctb(i));
elseif est_mach == 1.46;
    alpha(i) = alpha1_46(i);
    beta(i) = beta1_46(i);
    Csa(i) = Csa1_46(i);
    Csb(i) = Csb1_46(i);
    Cs(i) = 0.5*(Csa(i) + Csb(i));
    Cta(i) = Cta1_46(i);
    Ctb(i) = Ctb1_46(i);
    Ct(i) = 0.5*(Cta(i) + Ctb(i));
elseif (est_mach > 1.46) && (est_mach < 1.69)
    Mh = 1.69;
    Ml = 1.46;

```

```

alpha(i) = alpha(i) + ((est_mach - Ml)/(Mh - Ml))*(alphah(i) - alpha(i));
beta(i) = betal(i) + ((est_mach - Ml)/(Mh - Ml))*(betah(i) - betal(i));
Csa(i) = Csal(i) + ((est_mach - Ml)/(Mh - Ml))*(Csah(i) - Csal(i));
Csb(i) = Csbl(i) + ((est_mach - Ml)/(Mh - Ml))*(Csbh(i) - Csbl(i));
Cs(i) = 0.5*(Csa(i) + Csb(i));
Cta(i) = Ctal(i) + ((est_mach - Ml)/(Mh - Ml))*(Ctah(i) - Ctal(i));
Ctb(i) = Ctbl(i) + ((est_mach - Ml)/(Mh - Ml))*(Ctbh(i) - Ctbl(i));
Ct(i) = 0.5*(Cta(i) + Ctb(i));
elseif est_mach >= 1.69
alpha(i) = alpha1_69(i);
beta(i) = beta1_69(i);
Csa(i) = Csa1_69(i);
Csb(i) = Csb1_69(i);
Cs(i) = 0.5*(Csa(i) + Csb(i));
Cta(i) = Cta1_69(i);
Ctb(i) = Ctb1_69(i);
Ct(i) = 0.5*(Cta(i) + Ctb(i));
end

%-----
% Calculate Static & Total Pressures
%-----
Psa(i) = P1 - Csa(i)*pQBAR;
Psb(i) = P1 - Csb(i)*pQBAR;
Ps(i) = 0.5*(Psa(i) + Psb(i));

Pta(i) = P1 - Cta(i)*pQBAR;
Ptb(i) = P1 - Ctb(i)*pQBAR;
Pt(i) = 0.5*(Pta(i) + Ptb(i));

%-----
% Calculate Mach Number & Check for Convergence
%-----
macha(i) = ((2/(gamma-1))*(((Pta(i)/Psa(i))^(gamma-1)/gamma) - 1))^0.5;
machb(i) = ((2/(gamma-1))*(((Ptb(i)/Psb(i))^(gamma-1)/gamma) - 1))^0.5;
mach(i) = 0.5*(macha(i) + machb(i));
est_mach = mach(i);

%-----
% Output Final Solutions
%-----
if i > 1
dm(i,1) = ((mach(i) - mach(i-1))/mach(i))*100;
if abs(dm(i,1)) > 0.01
stop = 0;
else
stop = 1;
iter = length(mach);
alpha = alpha(end);
beta = beta(end);
Cs = Cs(end);
Ct = Ct(end);
Ps = Ps(end);
Pt = Pt(end);
MACH = mach(end);
QBARa = 0.5*gamma*Psa(end)*macha(end)^2;

```

```
QBARb = 0.5*gamma*Psb(end)*machb(end)^2;  
QBAR = (0.5*(QBARa(end) + QBARb(end)))*144;  
stop = 1;  
end  
end  
i = i + 1;  
end
```

Acknowledgements

I would like to thank my supervisor and branch chief, Jennifer Cole for allowing me the opportunity to work in the Aerodynamic & Propulsion Branch for the Spring 2011 term. In addition, I would sincerely want to thank my Cooperative Education Experience mentor and senior project industry advisor, Mike Frederick for all of his help and advice throughout the duration of my project. Also, I want to thank my school advisor, Dr. Eric Mehiel, head of Cal Poly San Luis Obispo's Aerospace Engineering Department for monitoring my progress during my stay here at NASA DFRC. Furthermore, I would like to thank the entire staff at NASA Dryden Flight Research Center and the F-15B Project Team for making my stay here over the past two years an enjoyable and educational experience. Finally, I want to thank the most important people in my life, my parents and my sister, for their unending support throughout my college education.

References

- [1] Weir, Lois J., Sanders, Bobby W., Meleason, Edward T., and Podleski, Steve D., "Flight Testing of a New Design Concept for Axisymmetric Inlets," TechLand Research, Inc., TechLand Research Report Number TRR-020406, North Olmsted, OH, Feb. 2006.
- [2] Weir, Lois J., Sanders, Bobby W., and Vachon, Michael J., "A New Design Concept for Supersonic Axisymmetric Inlets," AIAA-2002-3775.
- [3] Frederick, Mike, and St. John, Clint, "Propulsion Flight Test Fixture (PFTF): Channeled Centerbody Inlet Experiment (CCIE) – Flight Tests of the Channeled Centerbody Inlet Concept, Objectives and Requirements Document (ORD), F-15B Project," NASA CCIE ORD Rev. 6, Edwards, CA, Feb. 2011.
- [4] & [15] Andrews, Mark F., Abernathy, Michael, and Pritchett, Victor, "Calibration of Mach Number Set Points for the MSFC 14 × 14-Inch Trisonic Wind Tunnel," Report No.: ESTSG-FY10-01636, Jacobs Engineering, Ducommun Miltec, and NASA, May 2010.
- [5] "Dryden 5-Hole Probe Test Brief," NASA DFRC, Edwards, CA, Jun. 2010.
- [6], [9] & [10] Zeiger, Matthew D. and Schaeffler, Norman W., "Correcting Multi-Hole Probe Alignment Bias Errors Post-Calibration," Aeroprobe Corporation, Blacksburg, VA, AIAA-2001-0900.
- [7] & [13] Centolanzi, Frank J., "Characteristics of a 40° Cone for Measuring Mach Number, Total Pressure, and Flow Angles at Supersonic Speeds," NACA TN 3967, May 1957.
- [8] Zeiger, M. D., Chalmers, L. P., and D. P. Telionis, "Tip Geometry Effects on Calibration and Performance of Seven-Hole Probes," Aeroprobe Corporation & Virginia Polytechnic Institute and State University, AIAA-1998-2810.
- [11] Anderson, John D., *Fundamentals of Aerodynamics*, 5th edition, McGraw-Hill, New York, 2011, pp.826-827.
- [12] John, James E. and Keith, Theo G, *Gas Dynamics*, 3rd Edition, Pearson Prentice Hall, Upper Saddle River, NJ, 2006, pp. 82 - 88.
- [14] Ames Research Staff, "Equations, Tables, and Charts for Compressible Flow," NACA Report 1135, 1953.